

## Journal of Rehabilitation in Civil Engineering

Journal homepage: https://civiljournal.semnan.ac.ir/

# Retrofitting Seismically Designed Exterior Beam-Column Joints under Lateral Monotonic Loading: A Numerical Analysis Based on Experimental Testing

# Ali Mohammed Owaid <sup>1</sup>, Amir Houshang Akhaveissy <sup>2</sup>, Bahaa Hussain Al-Abbas <sup>3</sup>

- 1. Ph.D. Candidate, Department of Civil Engineering, Faculty Engineering, Razi University, Kermanshah, Iran
- 2. Associate Professor, Department of Civil Engineering, Faculty Engineering, Razi University, Kermanshah, Iran
- 3. Assistant Professor, Department of Civil Engineering, Faculty Engineering, Kerbala University, Kerbala, Iraq Corresponding author: *Ahakhaveissy@razi.ac.ir*

## **ARTICLE INFO**

#### Article history:

Received: 25 April 2024 Revised: 21 January 2025 Accepted: 24 January 2025

#### Keywords:

Exterior beam column joints; Peak monotonic load; Reinforced concrete; Retrofitting numerical model; Energy dissipation.

#### **ABSTRACT**

This research paper presents an experimental and numerical study on the behavior of reinforced concrete (RC) in exterior beamcolumn joints designed for seismic conditions. Three laboratory specimens were prepared and tested to evaluate their load-bearing capacity and study the joint behavior under a constant axial load and a gradually increasing peak monotonic load until failure. The demonstrated experimental results convergence specimens in terms of the load-displacement curve, displacement ductility, and energy dissipation. This was further confirmed through the use of a Finite Element (FE) analysis model. The analysis exhibited significant convergence experimental and numerical results. Additionally, the numerical model was retrofitted using Carbon Fiber Reinforced Polymer (CFRP) in two methods: model 1 (CFRP sheets only) and model 2 (CFRP sheets with strips). The retrofitting with CFRP proved for enhancing structure performance, improvement in failure mode and a significant increase in peak monotonic load and energy dissipation by (31 and 26) % for model 1, and by (47 and 36) % for model 2. This provides valuable insights into the behavior of RC exterior beam-column joints, highlighting the importance of retrofitting with CFRP composites.

E-ISSN: 2345-4423

© 2025 The Authors. Journal of Rehabilitation in Civil Engineering published by Semnan University Press. This is an open access article under the CC-BY 4.0 license. (https://creativecommons.org/licenses/by/4.0/)

#### How to cite this article:

Owaid, A. Mohammed, Akhaveissy, A. Houshang and Al-Abbas, B. Hussain (2026). Retrofitting Seismically Designed Exterior Beam-Column Joints under Lateral Monotonic Loading: A Numerical Analysis Based on Experimental Testing. Journal of Rehabilitation in Civil Engineering, 14(1), 2043 https://doi.org/10.22075/jrce.2024.33704.2043

### 1. Introduction

## 1.1. Background

The concrete connections between the column and the beam are critical and sensitive points in reinforced concrete structures [1]. The main task of these connections is to transfer all bending and torsional moments, as well as axial and lateral forces between the connected members [2]. Before the 1970s, due to a lack of understanding of the proper behavior of concrete connections between the column and the beam, there were no specific regulations for their design [3]. During that period, it was believed that after evaluating the stresses in the members adjacent to the connection, there was no need to control the stress in the core of the connection, which is usually larger than the cross-sectional area of the beam and column. Through the analysis of structures damaged by numerous earthquakes worldwide, the main cause of structural damage was identified as the failure of the structural unit in the connection and weakness in this area [4]. The structural joint between the beam and column, also known as the beam-column connection, is subjected to seismic forces during earthquakes. These forces are caused by the weight of the structure and the horizontal movement of the earthquake. If this critical joint fails, it poses a risk of compromising the structural integrity of the entire building and ultimately leading to its collapse. Therefore, it is crucial to ensure the strength and stability of this joint to prevent potential damage [5-7]. Rehabilitating and retrofitting reinforced concrete buildings damaged by seismic activity has become a fundamental issue in the field of structural engineering [8]. In the last two decades, there has been a significant amount of research focused on rehabilitating vulnerable beam-column joint connections. As a result, several methods have been proposed to enhance their performance [9,10]. In the realm of reinforced concrete and masonry structure enhancement, promising new techniques are emerging. These techniques place a focus on employing advanced materials and alternative methods, such as the application of external cladding and coatings utilizing high-performance composite materials. One such material that has garnered significant attention is carbon fiber-reinforced polymer (CFRP) [11–14]. In the last two decades, CFRP has been widely used and studied advantages, such its numerous as its ease implementation and quick application. Furthermore, this material has shown strong resistance to corrosion, a favorable strength-to-weight ratio, high stiffness, and low density [15–17]. Consequently, CFRP has emerged as a highly popular and credible material in the modern era for strengthening and enhancing the performance of diverse structural components, such as beams [18,19], columns [20,21], beam-column connections [22,23], and numerous other elements [24].

## 1.2. Literature review

Several studies have shown that the use of materials in the form of paper, strips, layers, and laminates has proven to be effective as a rapid assembly, easy-to-apply, safe, and reliable technique for enhancing and repairing structures. Researchers have investigated the effectiveness of these applications in improving the overall performance of structures made of reinforced concrete [25–27]. Akguzel and Pampanin [28] proposed a design methodology for retrofitting RC beam-column joints against seismic activity using FRP composites. In other study, T. Tafsirojjaman et al. [29] studied the performance of square hollow section (SHS) beam-column connections strengthened with externally bonded CFRP and glass fiber reinforced polymer (GFRP) under sustained monotonic and cyclic loading. The results showed promising improvements in joint behavior, energy dissipation, and ductility for both types of loading. In other study, Sarmad A. Ali and John P. Forth [30] explored the experimental and analytical behavior of exterior beam-column connections, where they were reinforced using different CFRP jackets on the beam only, under the effect of combined monotonic loading. The results showed a significant increase in the failure load due to the maximum stresses generated in these reinforced connections, leading to a sudden brittle failure. The finite element (FE) method is widely used due to its benefits, such as time and cost efficiency, as well as its

ability to analyze structures at a full scale. This method is commonly employed to model entire (RC) buildings in FE software, making the analysis particularly powerful, especially in the context of progressive collapse. FE models, implemented through commercial software, enable a more accurate and reliable simulation of the response of RC structures under different progressive collapse scenarios. Furthermore, these models are instrumental in exploring a variety of design variables, enhancing the overall versatility of the analysis [31]. Ciro Del V. et al. [32] investigated the capability of nonlinear Finite Element (FE) analysis to estimate the seismic responses of reinforced concrete (RC) beam-column connections that were strengthened using externally bonded CFRP under either monotonic or cyclic loading. The CFRP was applied to the top and bottom sides of the beam. The numerical results were accurate compared to the experimental findings in terms of the load-displacement curve and failure mechanisms. Recently, A. Dalalbashi et al. [33] conducted a numerical investigation on the effectiveness of CFRP sheets in improving the seismic performance of reinforced concrete (RC) beam-column joints under the effect of combined axial and cyclic loads by strengthening a set of connections using three different external strengthening configurations (L-shape, grid reinforcement, and flange reinforcement). The numerical analysis of the strengthened models showed clear convergence with the experimental samples in terms of the beam-end load versus beam-end displacement, energy dissipation, and plastic hinge formation. The results confirmed that the strengthened connections showed improved load-carrying capacity for all strengthening methods. In other study, Ahmad G. Saad et al. [12] presented a two-dimensional nonlinear model to investigate the lateral separation behavior of non-seismic RC beam-column joints strengthened extensively using CFRP. It also proposed new design equations to calculate the separation force for CFRP-strengthened beamcolumn joints. The results showed that the developed design equations were capable of estimating the separation forces for CFRP-strengthened beam-column joints through comparison with experimental work and model results. Kianosh Farhang et al. [22] conducted a numerical investigation using the Abaqus program and an experimental investigation on the shear strengthening of three-dimensional exterior beamcolumn joints that lack reinforcement in the joint core, under the influence of combined gravity and reversed lateral loads. The results showed that the strengthened specimens exhibited increased lateral load capacity, energy dissipation, and prevented column shear failure compared to the unstrengthened specimens. Morankar et al. [34] presented an analysis and strengthening of beam-column joints using carbon materials in the ANSYS program. The results of the study showed significant improvements in the beam-column joints after the strengthening process. The use of carbon composite wraps reduces the deformation and increases the maximum principal stress in the different reinforcement patterns, confirming the effectiveness of the CFRP strengthening process. In other study, Jinyan Wang [35] performed a numerical analysis to investigate the post-fire seismic characteristics of reinforced concrete frame joints reinforced with CFRP under low-cycle reciprocating loads. The study revealed that the bearing capacity of the CFRP-reinforced joints remained almost unchanged after the fire, compared to unreinforced joints, during the elastic phase.

## 1.3. Research gap

Despite numerous studies addressing the reinforcement of beam-column joints using CFRP, further research is needed to compare laboratory specimens with numerical models. The gap lies in analyzing the performance of exterior beam-column joints under different variables, such as support methods, dimensions of the column and beam sections, lateral loading, and proposed numerical repair methods using CFRP materials.

#### 1.4. Objectives

This study aims to analyze the parameters of the exterior beam-column joint region in three specimens designed with similar geometry to withstand seismic activity. The study will compare the behavior of laboratory specimens with numerical models to validate their accuracy. The study will propose the use of

CFRP materials as a method to strengthen the damaged area in the beam-column joint. These materials are known for their high strength-to-weight ratio and corrosion resistance, making them a popular choice for improving the load capacity and structural strength of concrete structures. The study aims to enhance joint performance while reducing economic costs and minimizing risk in the joint region by shifting it to the beam region. Fig. 1 represents a flowchart of the research process.

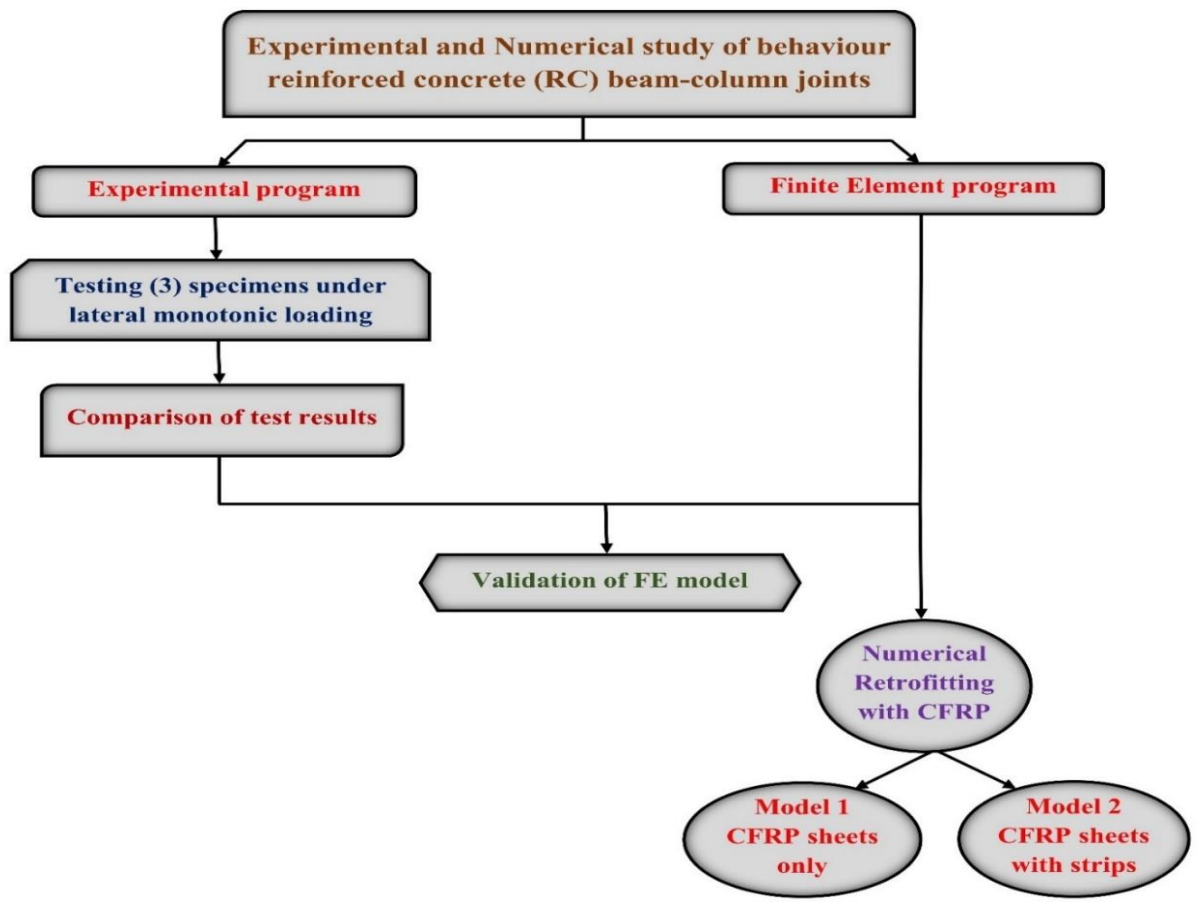


Fig. 1. Flowchart of the research process.

# 2. Experimental program

## 2.1. Design, dimensions, and reinforcement details for beam-column joint specimens

The experiment includes three specimens that replicate the exterior beam-column joint in the testing program. Specimens representing an exterior beam-column joint were designed to simulate a multi-story structural building regardless of the number of floors and the dimensions and details of the building. The dimensions of the specimens were selected according to the requirements and capacities of the testing equipment available at the University of Karbala, College of Engineering, Iraq. Three samples of exterior RC beam-column joints were cast, as shown in Fig. 2. The cross-section of the beams had dimensions of (200 x 190) mm and a length of (570) mm, extending to the column face. The cross-section of the columns had dimensions of (250 x 190) mm and a total height of (860) mm. The main reinforcement for beams and columns was (10) mm in diameter, and the transverse reinforcement for columns and beams was (6) mm in diameter with a spacing of (40) mm C/C. The reinforcement detailing for all samples followed the guidelines of ACI (352R-02 and 318-14) [36,37]. Fig. 3 displays the schematic diagrams of the three specimens, including reinforcement details and dimensions. The reinforcement steel bars with diameters of (6 and 10) mm were tested in the laboratory of the University of Babylon. Table 1 shows the physical properties of the reinforcement steel bars according to (ASTM A615/A615M-15) [38].



Fig. 2. Beam-column joints specimens.

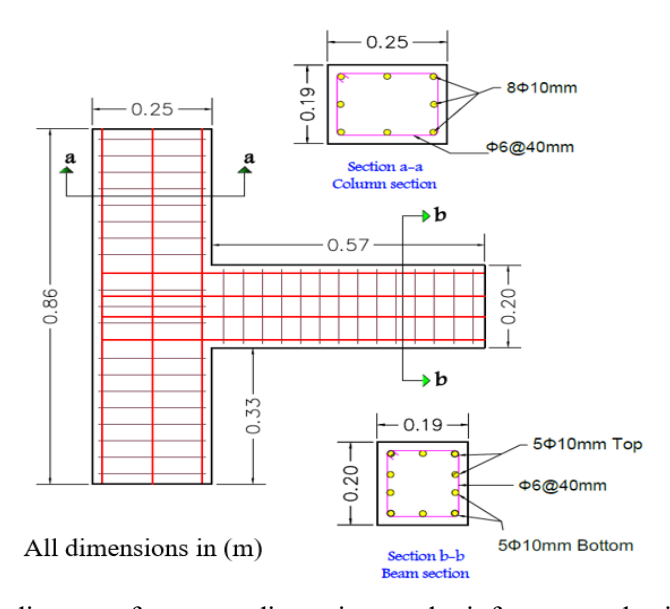


Fig. 3. A schematic diagram of concrete dimensions and reinforcement details for specimens.

**Table 1.** Physical properties of steel bars.

	Cross				
Diameter of bars (mm)	sectional area, (mm²)	Yield strength (MPa)	Tensile strength (MPa)	Maximum tensile strain (%)	Elastic modulus (GPa)
6	28.26	285	415	8	198
10	78.50	310	420	8	200

#### 2.2. Materials

The specimens were cast using laboratory-manufactured normal concrete with a compressive strength of (25) MPa. The concrete mix design in this paper conducted in accordance with the American Concrete Institute (ACI) (211.1-91) [39]. Table 2 presents mix proportions concrete for (1) m³. Three standard cylinders with an average compressive strength of (25.6) MPa and three standard cylinders with an average tensile strength of (2.0) MPa for the concrete mix were tested in the laboratory of the University of Babylon. Table 3 presents the cylindrical compressive and tensile strengths of the concrete specimens. The ordinary Portland cement (OPC) type (I) was used in the study supplied from Sulaymaniyah, Iraq, in accordance with (ASTM C150-07) [40]. The ratio of cement, fine aggregate, coarse aggregate is (1:1.89:2.77) with the water/cement ratio (0.48). The fine aggregate in the concrete mix consisted of natural sand obtained from

Karbala, Iraq, with a fineness modulus of (2.8), while the coarse aggregate crushed type from Baghdad, Iraq, with a size of (9.5) mm and a specific gravity of (2.58) were used, in accordance with (ASTM C33-16) [41]. Drinking water suitable for concrete mixing operations was used. To enhance workability with a minimal water content, a superplasticizer admixture commonly known as (Master Glenium-54) at a rate of (1%) by weight of the cement was used, in accordance with (ASTM C494-05) [42]. A Slump quantity of (75-100) mm was determined for normal concrete according to (ASTM C143-05) [43]. Table 4 provide the properties of the materials used in the experimental program.

**Table 2.** Mix proportions concrete for (1) m<sup>3</sup>.

	Ingredient	Quantity (kg/m³)
ength	Cement	350
<u> </u>	Water	168
Designed ressive sti (25) MPa	Water/Cement	0.48
Desi ressi (25)	Fine aggregates	700
De ompres	Coarse aggregate	1025
Cor	Super plasticizer	3.5

**Table 3.** Cylindrical compressive and tensile strengths of concrete specimens.

Specimen	Density (kg/m³)	Avg. (kg/m³)	Compressive Strength (MPa)	Avg. (MPa)	Tensile Strength (MPa)	Avg. (MPa)
S.1	2375		25.6		2.1	
S.2	2405	2388	25.3	25.6	1.9	2.0
S.3	2385		26.1		2.0	

**Table 4.** Physical properties of fine aggregates and coarse aggregates.

	<del>00 0</del>	88 8
Characteristics –	Fine aggregate	Coarse aggregate
Characteristics	Test value	Test value
Maximum nominal size (mm)	4.75	9.5
Unit weight (kg/m³)	1665	1530
Fineness modulus	2.80	6.25
Specific gravity	2.70	2.58
Total water absorption (%)	2.38	1.88
Туре	-	crushed

# 2.3. Boundary conditions of loading

In a moment frame structure under lateral load, the moments at mid-span of members are nearly zero. Therefore, if external connections are considered to represent a moment frame structure, the confinement conditions would be similar to those illustrated in Fig. (4-A). The bottom of the column has been designated with a hinge support, while the bottom of the beam is provided with a roller support. A typical quasi-static cyclic pattern and modeling setup were prepared for the tests in accordance with the "Commentary on Acceptance Criteria for Moment Frames Based on Structural Testing" (ACI T1.1-01) [44] and previous studies [45–49]. Fig. (4-B) illustrates a schematic diagram for the laboratory testing of the specimen, specifying the assigned boundary conditions for this study.

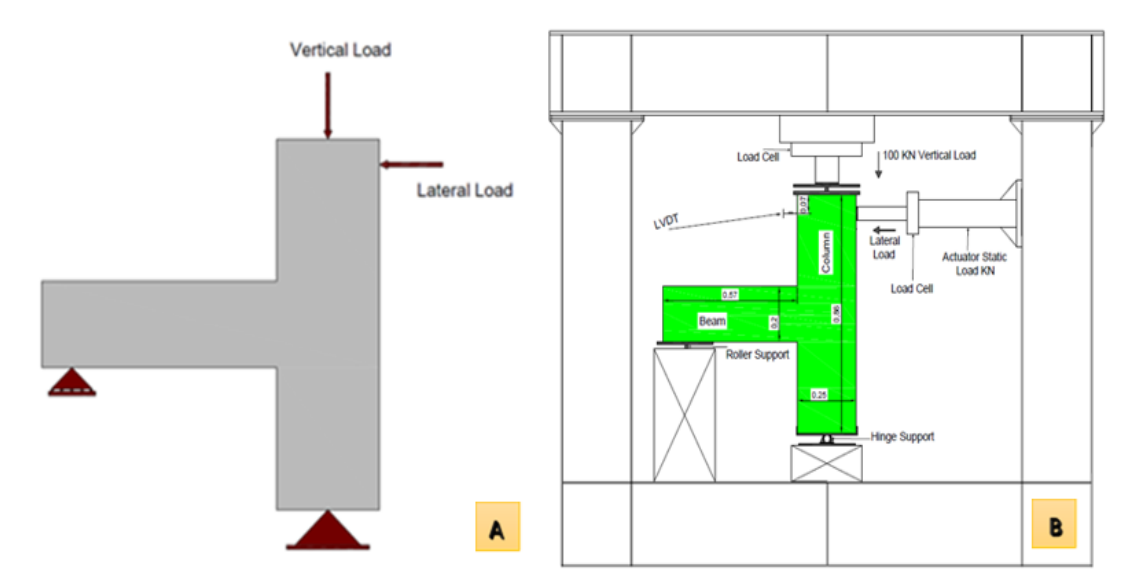


**Fig. 4.** A schematic diagrams: (A) boundary conditions in laboratory testing, (B) Test Set-up with Prototype Structure and Loading Protocol Sample.

## 2.4. Test procedure and instrumentation

The cyclic load has been extensively studied in previous research, but as a new experiment, the monotonic load was chosen to investigate the effect of seismic design improvement processes on concrete structures under such loading conditions. Cyclic loading is more representative of earthquakes, but monotonic static loading was chosen due to the available capabilities in the testing laboratory at the University of Kerbala. A constant axial load of (0.08\*Ac\*fc')=100 kN, where Ac represents the surface area of the column section, using a fixed load cell attached to a hydraulic jack, along with a lateral monotonic load in one direction positioned (70) mm away from the column face at the top, using a load cell attached to a horizontal jack, until complete failure occurred. The specimen was secured to the universal load structure through two support points. The first point involves a hinged support at the bottom of the column achieved by placing a base constrained from movement on excellently welded smooth reinforced steel bonded to the device structure. When applying axial load to the top portion of the column sample, the column compresses, thus preventing specimen movement. The second point supports the specimen from the beam side using a steel structure with a roller support positioned (70) mm away from the beam face to support the model during examination. The linear variable differential transformer (LVDT) was installed at one point: near the lateral monotonic load, positioned (70) mm away from the column face to measure displacement changes. Fig. 5 illustrates a picture of the setup and examination of the specimen in the laboratory.



Fig. 5. Picture of the test set-up and specimen in the laboratory.

After securing the model, axial and then lateral monotonic loads were applied sequentially and the displacement of the models at failure was measured. Load-Displacement curves were plotted for each specimen.

## 3. Results and discussions

#### 3.1. Peak monotonic load and failure mode

The table 5 shows the values of the first crack load ( $P_f$ ), displacement at first crack load ( $\delta_f$ ), peak monotonic load  $(P_p)$ , and displacement at peak monotonic load  $(\delta_p)$  for beam-column joint specimens subjected to monotonic lateral loading. Upon comparing the results of the laboratory samples, it can be observed that the first crack load values for the three specimens are relatively similar, with a difference percentage of (10%) between the highest and lowest values. This can be attributed to their similar geometric properties and loading conditions. The differences in peak monotonic load among the experimental specimens with symmetric dimensions and steel reinforcement do not exceed (5.4%). Although this percentage may seem small, it does not significantly affect the behavior and performance of the beam-column joint. However, there may be slight variations in the behavior of the concrete specimens due to differences in material distribution and compaction processes, which can affect the appearance and quantity of initial cracks for each model. The effect of displacement is also not significant. The failure of the specimens also exhibited brittleness, with flexural cracks initially appearing near the core area at the face of column on the external surface of the beams and then developing to the top surface. These cracks continued to appear with the increase in lateral loads. The flexural cracks extended to the top of the beams at the maximum load for each specimen. As the test proceeded, the flexural cracks widened, leading to spalling of the concrete at the top of the beams, which resulted in a decrease in load-bearing capacity, as shown in Fig. 6.

**Table 5.** Load and displacement at peak and First crack for the specimens.

Specimen designation	$P_{\rm f}(kN)$	$^{\delta}_{\mathrm{f}}(\mathrm{mm})$	P <sub>p</sub> (kN)	δ <sub>p</sub> (mm)
BCJ-1	18	2.5	54.3	39.6
BCJ-2	20	1.7	57.4	37.9
BCJ-3	20	2.6	56.2	38.0

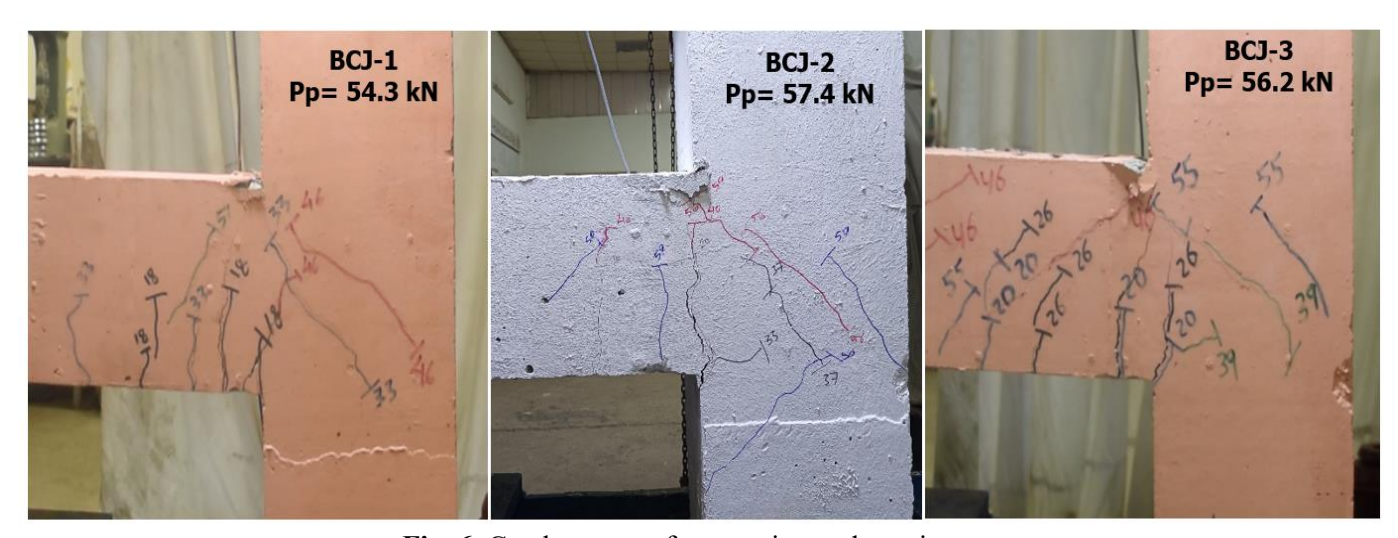


Fig. 6. Crack patterns for experimental specimens.

# 3.2. Load-displacement curve

The load-displacement curves of the beam-column joint specimens subjected to lateral monotonic loading are illustrated in Figure 7. The peak monotonic load and displacement values were recorded at a distance of 70 mm from the column face, using a load cell and load indicator for precise measurements. The curves for the specimens can be observed to be linear at the beginning of the loading, indicating that these reinforced concrete beam-column joints were still in the elastic stage. Due to the yielding of the reinforcement bars, the surface concrete of the specimens soon cracked, and flexural failure occurred at the end of the loading.

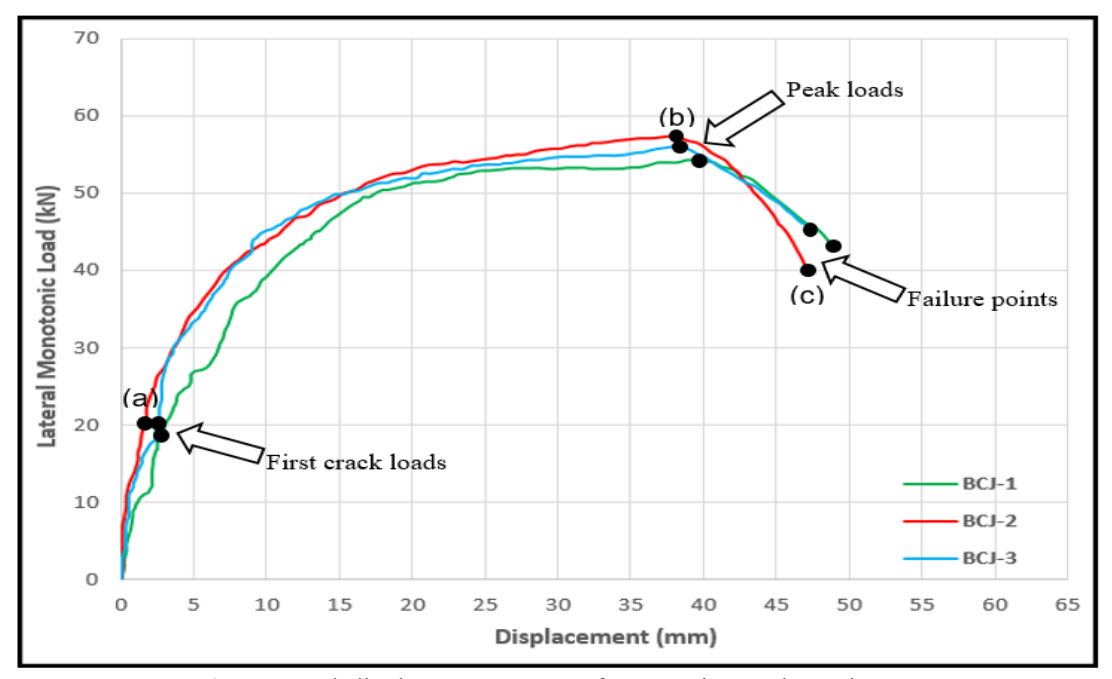


Fig. 7. Load-displacement curves for experimental specimens.

As shown in Figure 7, for specimen BCJ-2 absorbs the force in concrete from the loading moment to point (a). Stress in the concrete reaches the bending limit of the concrete at point (a), initiating cracking in the tension zone. From point (a) to point (b), the reinforcement can withstand the tensile force. The resistance value of the beam-column joint specimen approaches the ultimate load at point (b). Beyond point (b), bending increases significantly due to the yielding of the reinforcement, ultimately leading to failure at point (c).

## 3.3. Energy dissipation and stiffness

The energy dissipation ( $E_{diss}$ ) demonstrates the capacity and effectiveness of the specimens in absorbing and dissipating energy during lateral loading. A higher bending value indicates a greater ability of the exterior beam-column joint to resist seismic forces and reduce the risk of structural damage or failure. From the laboratory results, load-displacement curves were plotted for the specimens. Based on the load-displacement curves, the energy dissipation value was calculated, defined as the cumulative area under the load-displacement curve until final failure during plastic deformation in the beam-column joint specimens [49]. The  $E_{diss}$  is hence defined as the integral of the force displacement plot. Using the trapezoidal rule, this can be calculated from Eq. 1.

$$E_{diss} = \pi r^2 = \int_0^{\delta_{max}} P(\delta) \cdot d\delta \approx \sum_0^{\delta_{i+1} = \delta_{max}} \left( \left( \frac{P_{i+1} + P_i}{2} \right) x \left( \delta_{i+1} - \delta_i \right) \right)$$
 (1)

Where  $\delta_i$  and  $P_i$  are the measured lateral displacement and applied force, respectively, at each level of displacement, *i*. The stiffness (K) reflects the structure's response to lateral loads. A higher stiffness value means greater resistance to deformation and better structural stability. Through stiffness analysis, we can assess the ability of the exterior beam-column joint to resist lateral deformations and maintain the integrity of the structure. The stiffness of the joint, defined as the ratio of the Pp to  ${}^{\delta}p$ , The calculation was also performed [50,51]. The Stiffness (K) value is determined using Eq. 2.

$$K = \frac{Pp}{\delta_p} \tag{2}$$

**Table 6.** Experimental Results of cumulative energy dissipation and stiffness for specimens.

Specimen designation	P <sub>p</sub> (kN)	<sup>δ</sup> p (mm)	E <sub>diss</sub> (kN-mm)	K (kN/mm)
BCJ-1	54.3	39.6	1752	1.37
BCJ-2	57.4	37.9	1802	1.51
BCJ-3	56.2	38.0	1778	1.47

## 3.4. Displacement ductility

The extent of ductility is measured through a quantitative expression known as the ductility factor or ductility ratio. There are two distinct ductility factors: displacement ductility factor and curvature ductility factor. For the purposes of this study, the displacement ductility factor was utilized [51]. Table 7 provides information about  $(P_p)$ , yield load  $(P_y)$ , yielding displacement  $(^{\delta}_y)$ , effective ultimate displacement  $(^{\delta}_u)$  and ductility factor  $(\mu)$  for specimens. This is achieved due to the non-linear characteristics exhibited by the materials (steel reinforcement and concrete), leading to yielding at various locations and load levels. A technique for determining the yield point, relying on the idealized bilinear load—displacement response illustrated in Fig. 8 [52]. The yielding displacement is determined as the point at which the specimen fails or when the bearing capacity reduces to 85% of the peak load [53]. The ductility factor  $(\mu)$  is precisely defined as the ratio of the effective ultimate displacement to the yielding displacement, the ductility factor value is established by employing Eq. 3.

$$\mu = \frac{\delta_u}{\delta_v} \tag{3}$$

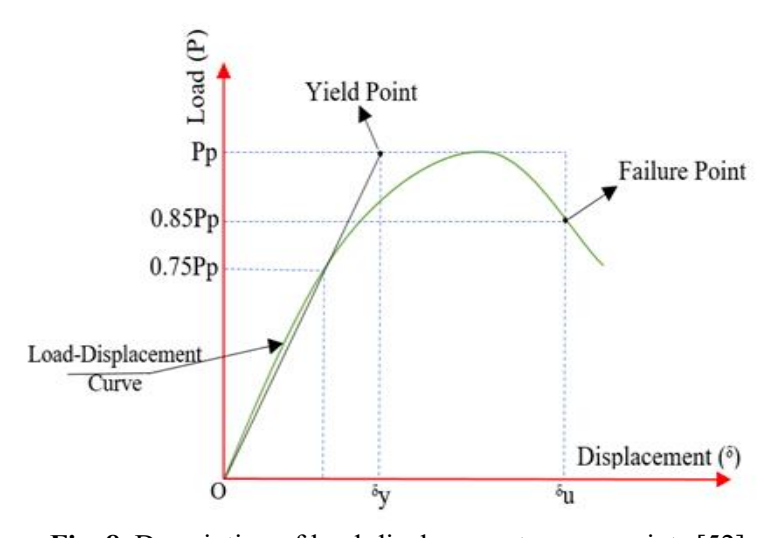


Fig. 8. Description of load-displacement curves points [52].

Table 7 represents the ductility factor ( $\mu$ ) for all specimens. The ductility factor values ranged from (3.3 to 3.9), with a difference percentage of (15.4%).

<b>Table 7.</b> Results of ductility factor f	for specimer	1S.

Specimen designation	$\begin{array}{c} P_p \\ (kN) \end{array}$	P <sub>y</sub> (kN)	δ <sub>γ</sub> (mm)	$P_{\mathrm{u}}^{}*}$ (kN)	δ <sub>u</sub> (mm)	μ
BCJ-1	54.3	46.2	14.2	46.2	47.2	3.3
BCJ-2	57.4	47.0	12.5	48.8	44.2	3.5
BCJ-3	56.2	47.0	11.8	47.8	45.8	3.9

Where:  $P_u$  (Ultimate load) = 85% \*  $P_p$ 

# 3.5. Numerical analysis of beam-column joints (Finite Element)

Numerical analysis was conducted using the Abaqus software to study the behavior of beam-column joints under monotonic loading. This process involved modeling the geometry of the specimens along with their materials such as concrete and steel, as well as loading and constraints. Additionally, it considered the interaction, impact, and connection between the materials. In Abaqus, the static general method was employed to simulate the finite element models. ABAQUS/CAE 2017 VERSION was used for modeling and analysis of beam-column joint.

## 3.5.1. Materials modelling

#### 3.5.1.1. Concrete

The Concrete Damaged Plasticity (CDP) model was chosen due to its capability and potential for modeling reinforced concrete and other quasi-brittle materials in various types of structures [54]. The (CDP) model can define the nonlinear behavior of the beam-column joint. Additionally, it considers isotropic damage elasticity concepts with isotropic tensile and compressive plasticity [55]. Reinforced concrete (RC) is composed of two main components - concrete and steel. Concrete exhibits significantly higher strength in compression compared to tension, with its tensile strength being approximately one-tenth of its compressive strength. The stress-strain relationship of concrete is markedly different between tension and compression. In tension, the relationship is nearly linear, whereas in compression, the stress-strain curve is nonlinear from the very start [56]. Several researchers have investigated and developed models for the nonlinear stressstrain behavior of concrete. Prominent among them are the works of Hognestad [57], Rusch [58], and Kaar [59]. In this study, the Hognestad model is employed to analyze the uniaxial behavior of concrete under pressure [60-62]. It also takes into account the degradation of elastic stiffness resulting from plastic straining in both compression and tension. The (CDP) model can exhibit the damage characteristics of a material. The primary failure mechanisms assumed by this model are tensile cracking and compressive crushing. Various parameters required in the (CDP) model were studied and selected based on available literature for both conventional and specific specimens. The dilation angle for the model was set at (56°). This angle is obtained due to a change in volumetric strain resulting from plastic shearing and depends on the internal friction angle. Table 8 represents the details of normal concrete properties and (CDP) parameters used in the Abaqus program.

Table 8. Normal concrete peoperties and CDP parameter.

	Table 6. Normal concrete peoperties and CD1 parameter	•
	Young's Modulus (E)	23.5 GPa
Normal Concrete	Poission's Ratio (υ)	0.2
Properties	Compressive Strength $(\sigma)$	25 MPa
	Specific Weight (SG)	$2400 \text{ Kg/m}^3$
	Dilation Angle (ψ)	56°
CDP Parameters	Eccentricity (e)	0.1
	$fb_0/fc_0$	1.16
	The second stress invariant/tensile meridian (K)	0.667
	Viscosity Parameter (μ)	0.001

## 3.5.1.2. Steel reinforcement

In Abaqus, experimental steel reinforcement (longitudinal bars and stirrups) can be represented based on two factors: the first being the bilinear stress-strain behavior and the second being the multilinear stress-strain behavior. The common practice assumes the use of multilinear stress-strain behavior due to the availability of sufficient information about stress and ultimate strain. Table 9 provides details about the experimental steel reinforcement in FE Model. The bonding in the embedded region for both the reinforcement and the concrete is assigned to achieve perfect connection [63]. The characteristics of the steel's behavior are well-defined, and any slippage between the steel rebar and concrete is disregarded, consistent with findings from prior research [64–67]. Sufficient development length of the reinforcement is assumed to accommodate friction in the experimental representation. The reinforcement is connected to the concrete through a defined interaction. The utilization of a two-line model for simulating the compressive and tensile characteristics of steel rebar's [68]. Fig. 9 illustrates the representation of reinforcement for the samples in both the experimental and the Abaqus software.

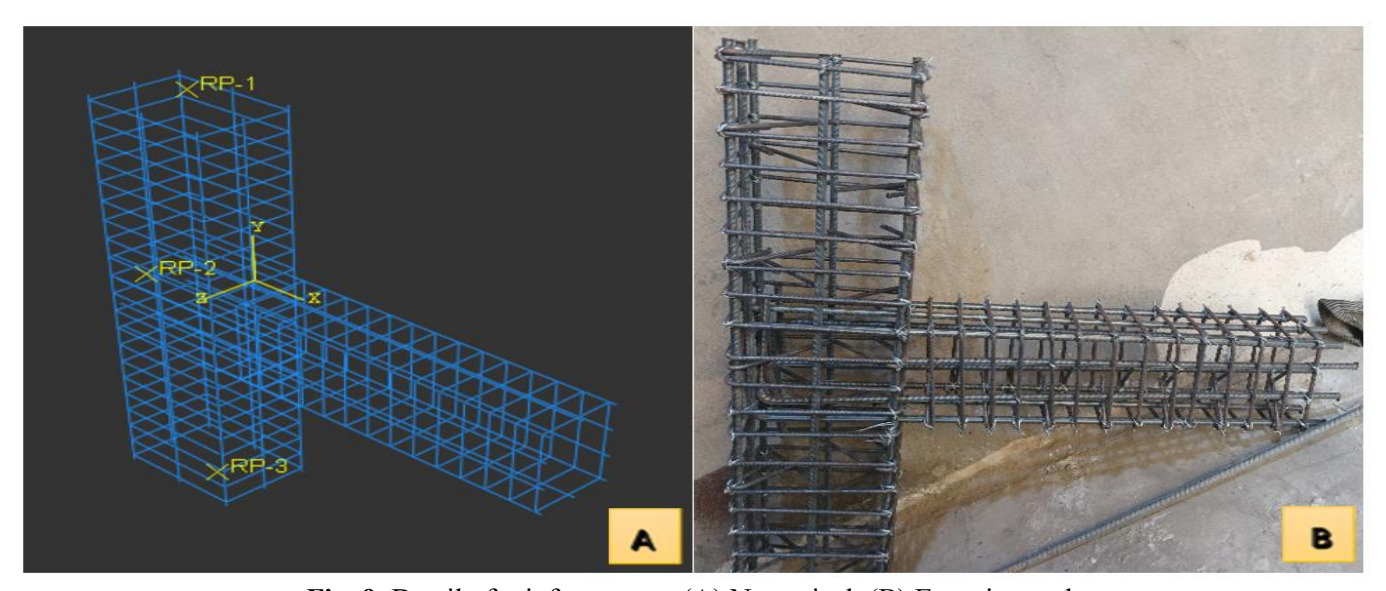


Fig. 9. Detail of reinforcement: (A) Numerical, (B) Experimental.

**Table 9.** Steel reinforcement peoperties.

Young's Modulus (E)	200 GPa
Poission's Ratio (υ)	0.3
Yield Strength	310 MPa
Ultimate Tensile Strength	420 MPa
Plastic strain	0.08
Specific Weight (SG)	$7800 \text{ Kg/m}^3$

## 3.5.2. Boundary conditions and loading

To achieve convergence between experimental and numerical simulations, samples were modeled in the Abaqus software with conditions that matched and were equivalent to the laboratory samples. To simulate the boundary conditions for the beam-column joint models, the bottom part of the column was constrained in both the X and Y directions, and the bottom part of the beam was constrained in the Y and Z directions. An axial load was applied to the column's surface (0.08\*Ac\*fc`), while lateral deformation was continuously and gradually applied to the top of the beam until the final failure of the sample, as illustrated in Fig. 10.

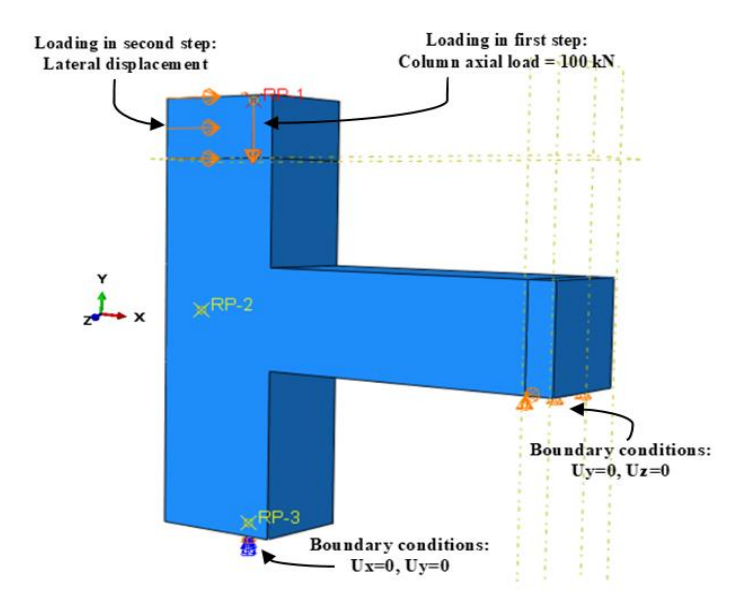
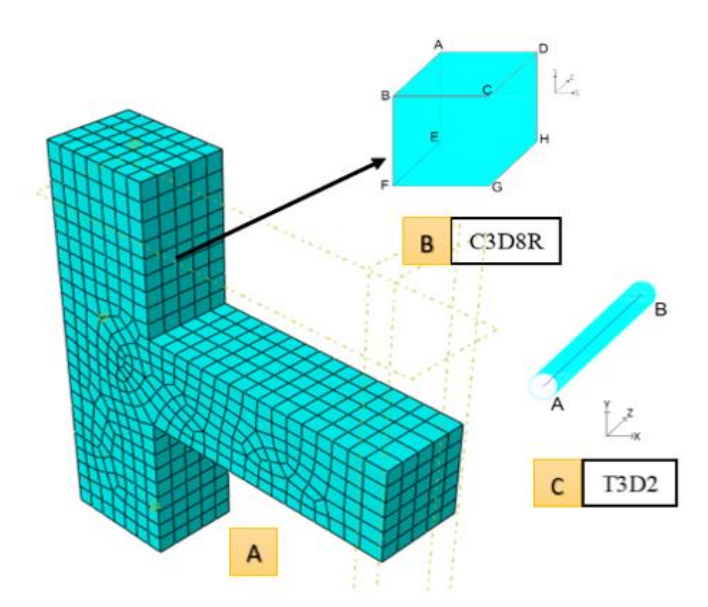


Fig. 10. Boundary conditions and loading in abaqus for specimen.

#### 3.5.3. Finite element mesh

For the purpose of obtaining accurate and realistic results, the beam-column joint specimens were simulated using 3D elements. Concrete was simulated by 8 nodded linear elements (C3D8R). The longitudinal and transverse reinforcement were modeled using 2 nodded liner truss elements (T3D2) in the resulting model. A mesh sensitivity analysis was conducted to determine the appropriate mesh size, where there are no significant changes in results with a smaller mesh. Mesh sizes of 50 mm, 45 mm, 40 mm, and 35 mm were examined for the concrete to find the suitable size. The model with a 50 mm mesh size is considered appropriate because it reduces analysis time compared to other sizes and provides results close to experimental findings. It should be noted that for the convergence of the analysis, the L2 norm for both force and displacement control is assumed to be equal to 0.005. The concrete mesh element size was set at (50) mm, while the longitudinal reinforcement mesh sizes were set at (80) mm, and the transverse reinforcement mesh size was set at (20) mm, as illustrated in Fig. 11.



**Fig. 11.** Finite Element Model: (A) Mesh, (B) Concrete solid element (C3D8R), (C) Sreel rebar truss element (T3D2).

## 3.5.4. Validation of experimental and numerical results

## 3.5.4.1. Energy dissipation and stiffness

Table 10 represent results of the (Pp), (8p), (Ediss) and (K) for the numerical model. When comparing the results at tables (6 and 10) between experimental samples and numerical analysis, it is observed that the peak load values for the numerical analysis varied within the range of the peak monotonic load values for the experimental samples. They decreased by (3.7%) from the highest value and increased by (1.8%) from the lowest value. As for the displacement at the peak monotonic load for the experimental samples, it decreased compared to the displacement of the numerical analysis by a percentage ranging between (3.4% - 7.6%). The Ediss percentage for the experimental samples decreased by a range of (8.5-11.0) % compared to the numerical analysis. In terms of stiffness, the numerical analysis decreased by a range of (1.5-10.6) % compared to the experimental specimens.

**Table 10.** Numerical Results of cumulative energy dissipation and stiffness for specimens.

Specimen designation	P <sub>p</sub> (kN)	<sup>δ</sup> p (mm)	E <sub>diss</sub> (kN-mm)	K (kN/mm)
Numerical analysis	55.3	41.0	1969	1.35

### 3.5.4.2. Load-displacement curves

The load-displacement curves for both the numerical analysis and experimental specimens are shown in Fig. 12. It can be seen that the initial stiffness of the numerical analysis is higher than that of the experimental specimens. This difference can be attributed to the lack of modeling for difficult hardening in the CDP model and simplifications made during the modeling process. This trend is also reported by several researchers [69,70]. However, as the displacement increases, the slope of the numerical analysis curve approaches that of the experimental specimen curve. Although there are slight variations in point-related displacements at peak load between the numerical analysis and experimental specimens, the numerical analysis accurately predicts the peak load. The highest peak load was observed in the experimental specimen (BCJ-2) with a value of (57.4 kN), while the predicted value for the peak load in the numerical analysis was (55.3 kN), showing a difference of (3.7%). The lowest peak load was observed in the experimental specimen (BCJ-1) with a value of (54.3 kN), which is only (1.8%) different from the predicted value in the numerical analysis. Overall, there is a satisfactory agreement between the numerical and experimental results, as shown by the percentage differences.

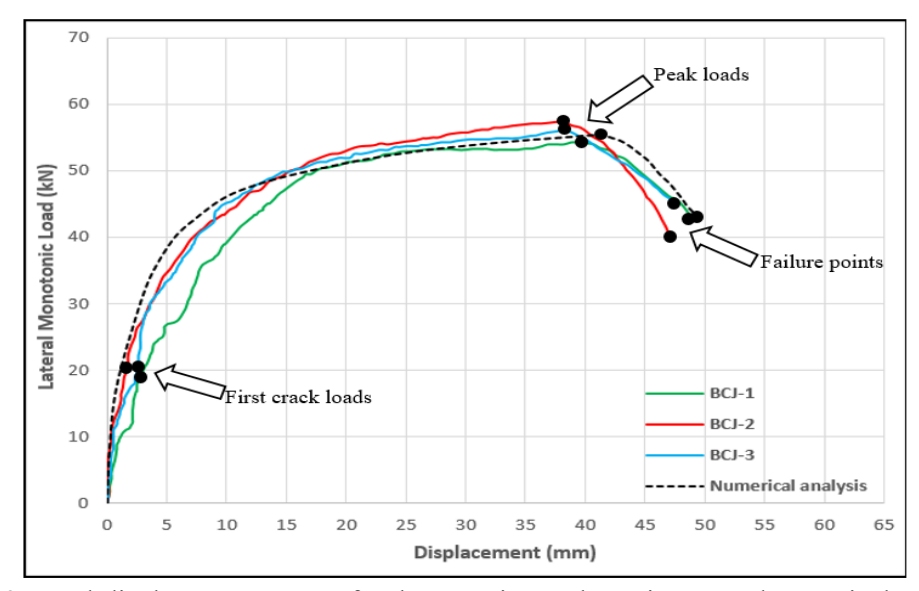


Fig. 12. Load-displacement curves for the experimental specimens and numerical analysis.

## 3.5.4.3. Displacement ductility

Table 11 presents the results for (Pp), (Py), ( $^{\delta}$ y), ( $^{\delta}$ u), and ( $\mu$ ) obtained from the numerical analysis. A comparison of the results from tables 7 and 11 reveals that the ductility factor values for the experimental specimens (3.3 and 3.9) are lower than the ductility factor value (5.3) obtained from the numerical analysis, with a decrease of 37.7% and 26.4%, respectively.

Tubic	11: Results of de	termity ractor	Tot i vaimeriear	anary Bib.		
Specimen	$P_p$	$\mathbf{P}_{\mathbf{y}}$	$^{\delta}\!y$	$P_{\mathrm{u}}$	$\delta_{u}$	ш
designation	(kN)	(kN)	(mm)	(kN)	(mm)	μ
Numerical analysis	55.3	44.5	8.9	47.0	47.5	5.3

**Table 11.** Results of ductility factor for Numerical analysis.

## 3.5.4.4. Cracking pattern

PEEQT refers to the tensile equivalent plastic strain [71]. Fig. 13 illustrates the PEEQT contour of the numerical model, showcasing both the cracking pattern and the mode of failure. In the numerical analysis, cracks initiate in the tensile zone at the bottom of the beam, then gradually expand to the upper compressive zone of the beam, reaching the beam-column joint. Flexural cracks appear on the face of the column. The failure in the experimental specimen is of a shear type, similar to the numerical model.

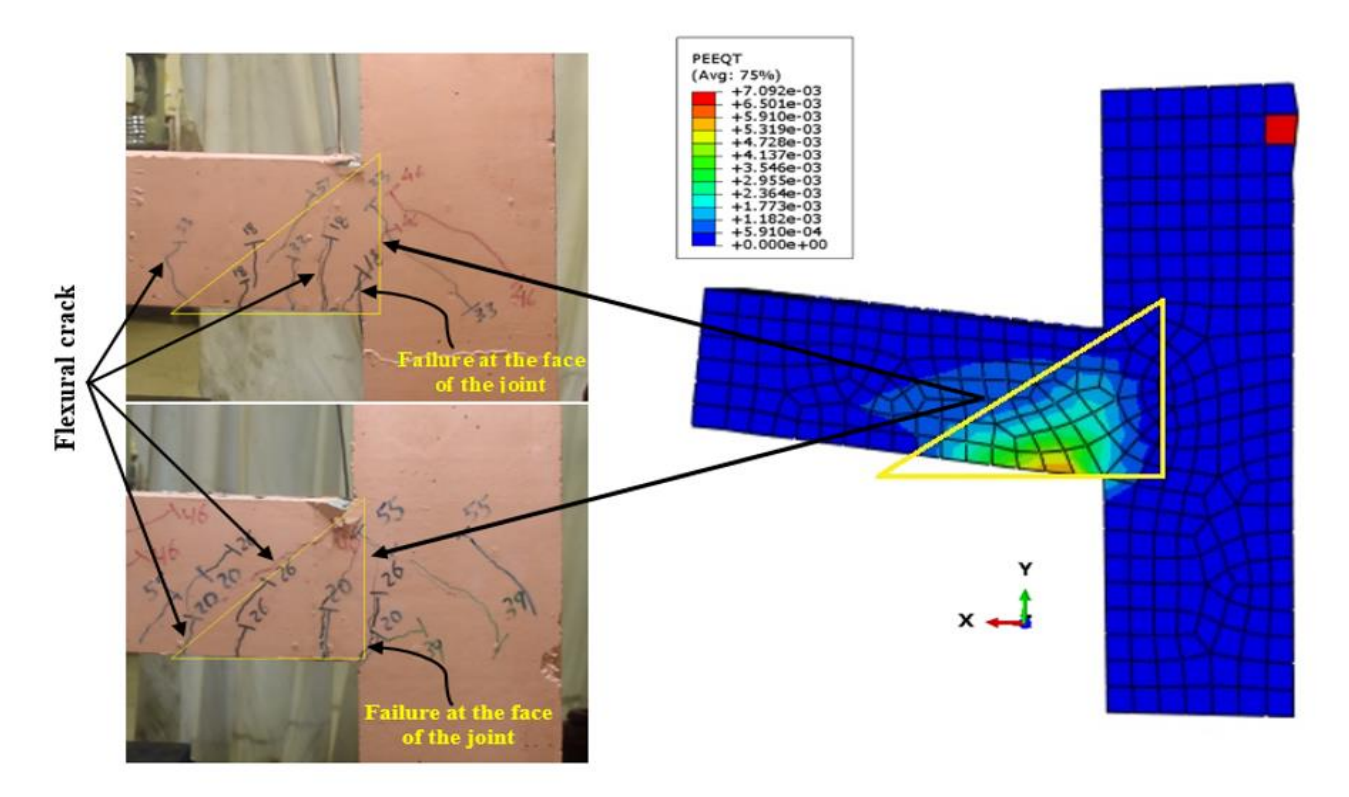


Fig. 13. Expected damage in specimens from FE-modelling (PEEQT) and observed experimental damage.

Fig. 14 illustrates the Von Mises stress contour, showing the state of reinforcement at the moment of failure for the numerical models. It is evident that the tensile reinforcements play a critical role in bearing the load. In the sample subjected to the force system, the reinforcement yields in the tension zone before the compression zone, indicating that this area has a higher capacity for bearing force. Furthermore, the stirrups undergo significant deformations before yielding, but they do not rupture.

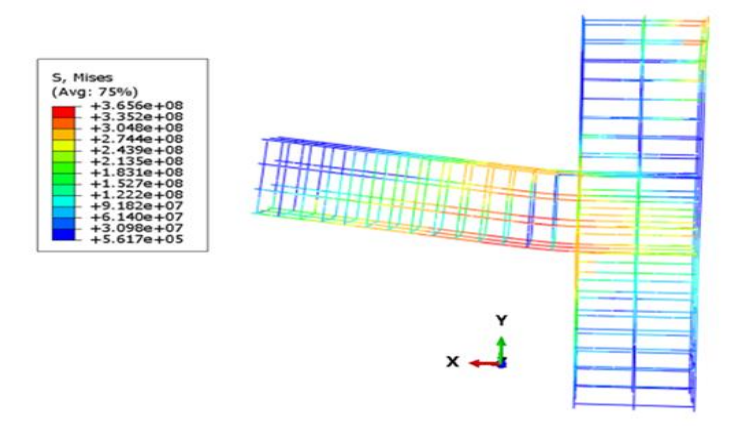


Fig. 14. Von Mises stress contour at the failure moment in numerical analysis.

## 3.6. Retrofitted joint

In this study, a suggestion for retrofitting the damaged of external beam-column joint due to external forces such as earthquakes, explosions, and others is inspired by Akhaveissy study [72]. The retrofit involves using carbon fiber-reinforced polymer (CFRP) instead of steel plates in two numerical models: the first model is retrofitted using CFRP sheets only, and the second model using CFRP sheets with strips. The aims to recover, enhance, and mitigate cracks in the critical beam-column joint. Fig. 15 represents the dimensions of the concrete and CFRP models. In characterizing the actual behavior of CFRP material, two different models are commonly employed. The first model considers the material as linear elastic and isotropic until failure, while the second model treats the material as linear elastic and anisotropic [73]. Since the material is manufactured unidirectional by the company, it is evident that its behavior is fundamentally anisotropic. In this model, the material is represented as unidirectional, where it is primarily subjected to stress in the fiber direction. Therefore, the elastic modulus in the fiber direction is considered the most crucial parameter, and for this reason, the model is considered entirely anisotropic. In this study, the elastic modulus in the fiber direction of the unidirectional CFRP material was used based on the manufacturer's data sheet as shown in table 12, specifying it as (112) GPa, with a Poisson's ratio of (0.3). By using rule of mixture,  $E_{11}$ = 112 GPa,  $E_{22}=E_{33}=82$  GPa,  $v_{11}=v_{22}=v_{33}=0.3$ ,  $G_{12}=G_{13}=4.5$  GPa,  $G_{23}=3$  GPa. Fig. 16 represents retrofitting of CFRP in Abaqus program.

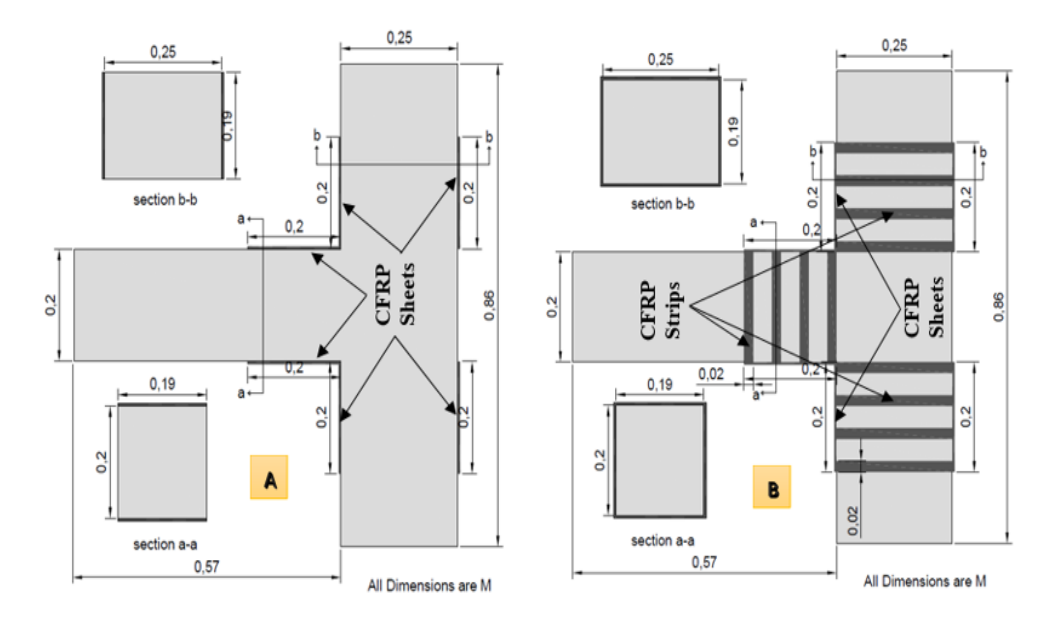


Fig. 15. A schematic diagram of dimensions for specimens with CFRP: (A) model 1, (B) model 2.

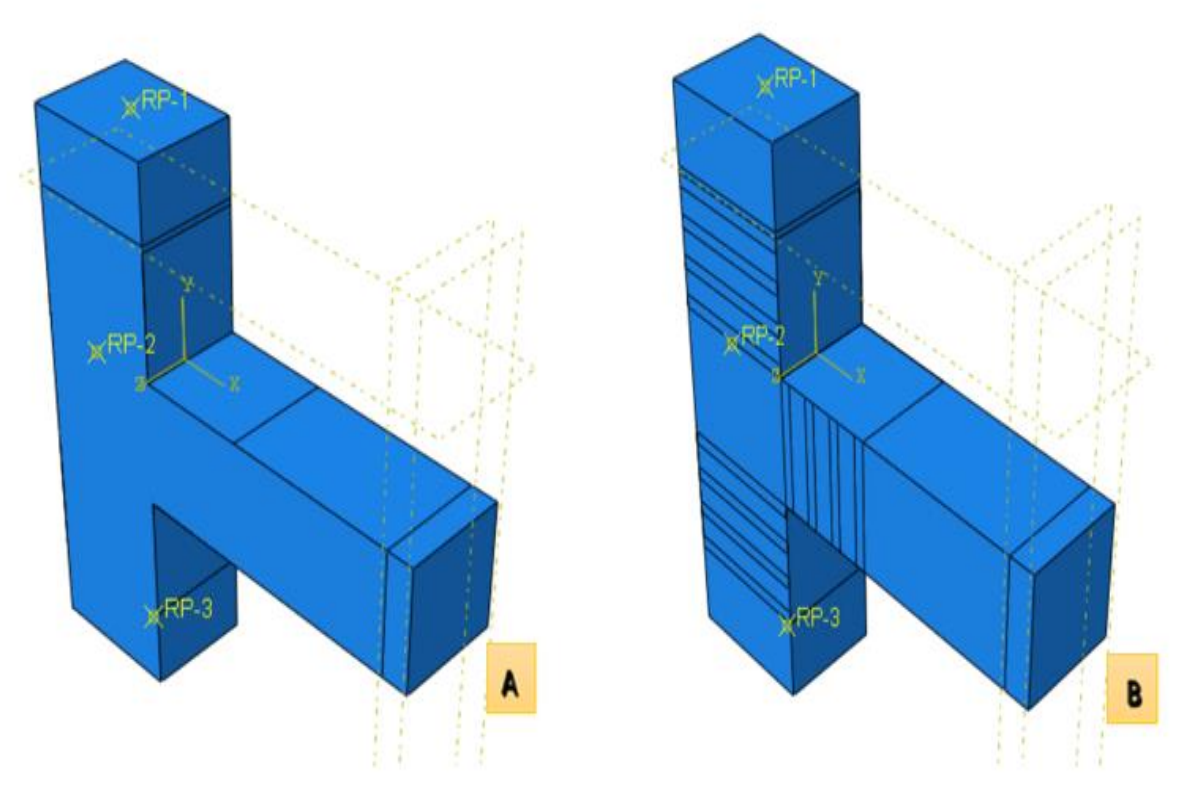


Fig. 16. Numerical models for retrofitting by CFRP: (A) model 1, (B) model 2.

S. No. Properties value Tensile Strength 1 4100 MPa 2 Tensile Elastic Modulus 2400 MPa 3 Elongation 1.60 % 4 1000 MPa Flexural Strength 5 80 MPa Shear Strength 6 Density 1.8 g/cm<sup>3</sup> 7 Fiber Thickness 1 mm

Table 12. Properties of CFRP fiber used for retroffiting.

#### 3.6.1. Model 1 (CFRP sheets only)

The numerical analysis of Model (1) illustrates the Von Mises stress contour at the failure moment and the PEEQT contour, as depicted in Figure 17. For the joint in Model 1, the benefits of using carbon fiber-reinforced polymer sheets were evident. By redirecting the damaged area from the near-column face to the beam end region at different levels along the strut, as illustrated in Fig. 17-A, the strength of the modified joint was increased. This improvement is attributed to the contribution of carbon fiber sheets in reinforcing both the column and beam joints and absorbing some of the forces before they penetrate into the concrete and reinforcement bars, enhancing tension reinforcement as shown in Fig. 17-B. The installation of CFRP sheets with dimensions of (190 x 200) mm achieved a significant improvement in the ultimate capacity of the joint, as depicted in Fig. 18.

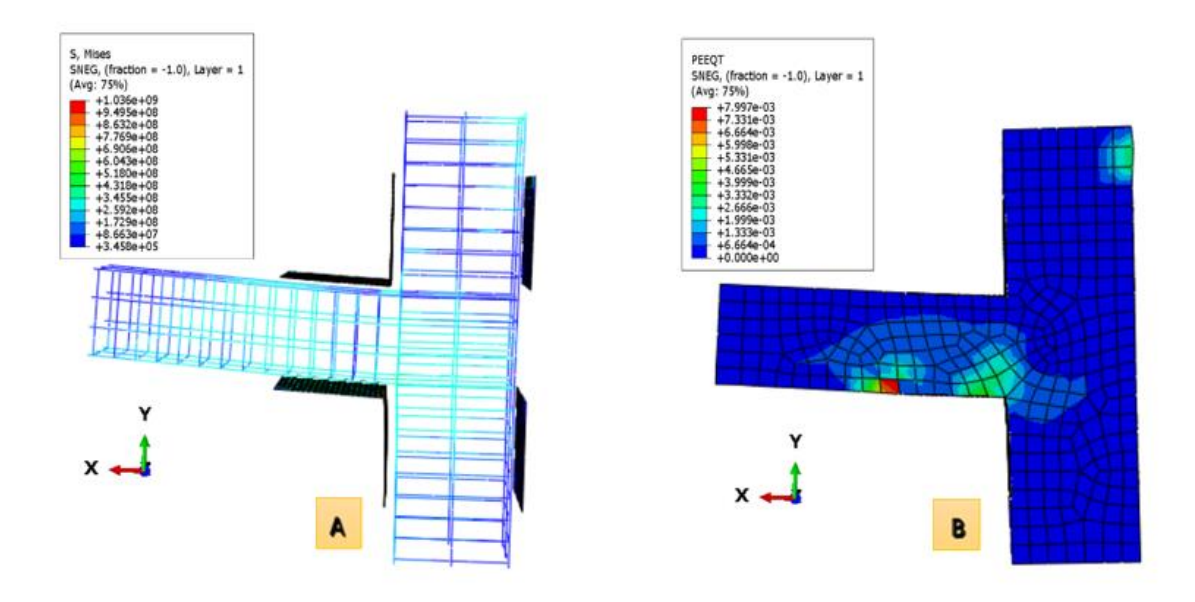


**Fig. 17.** Numerical retrofitting by CFRP for model 1: (A) Von Mises stress contour at the failure moment, (B) PEEQT contour.

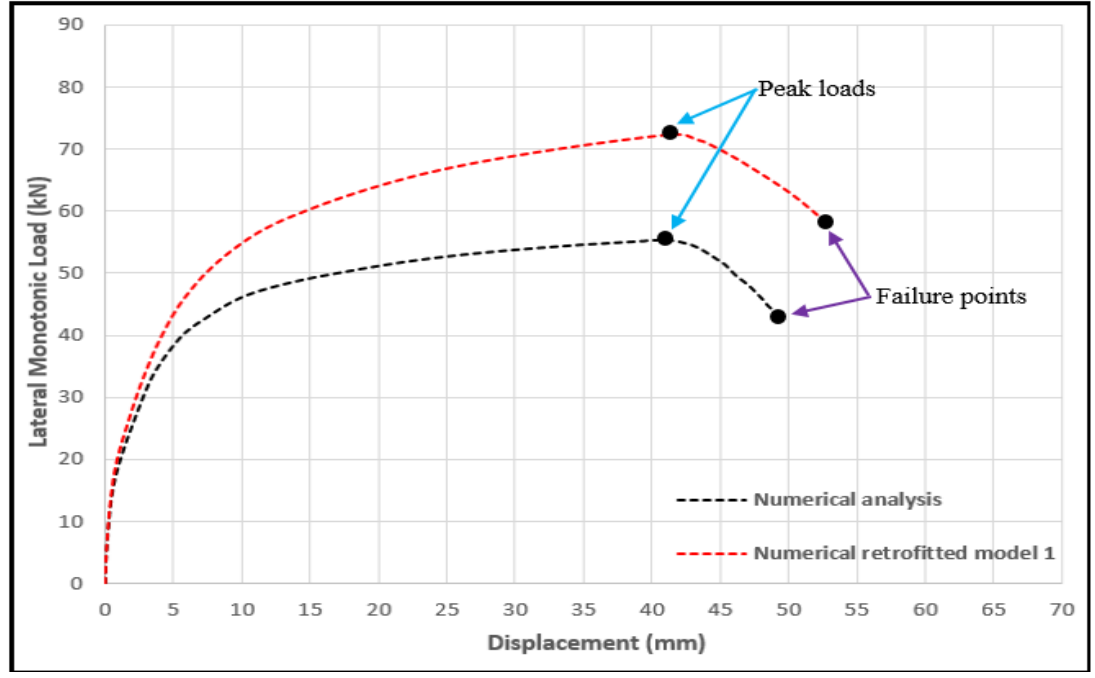
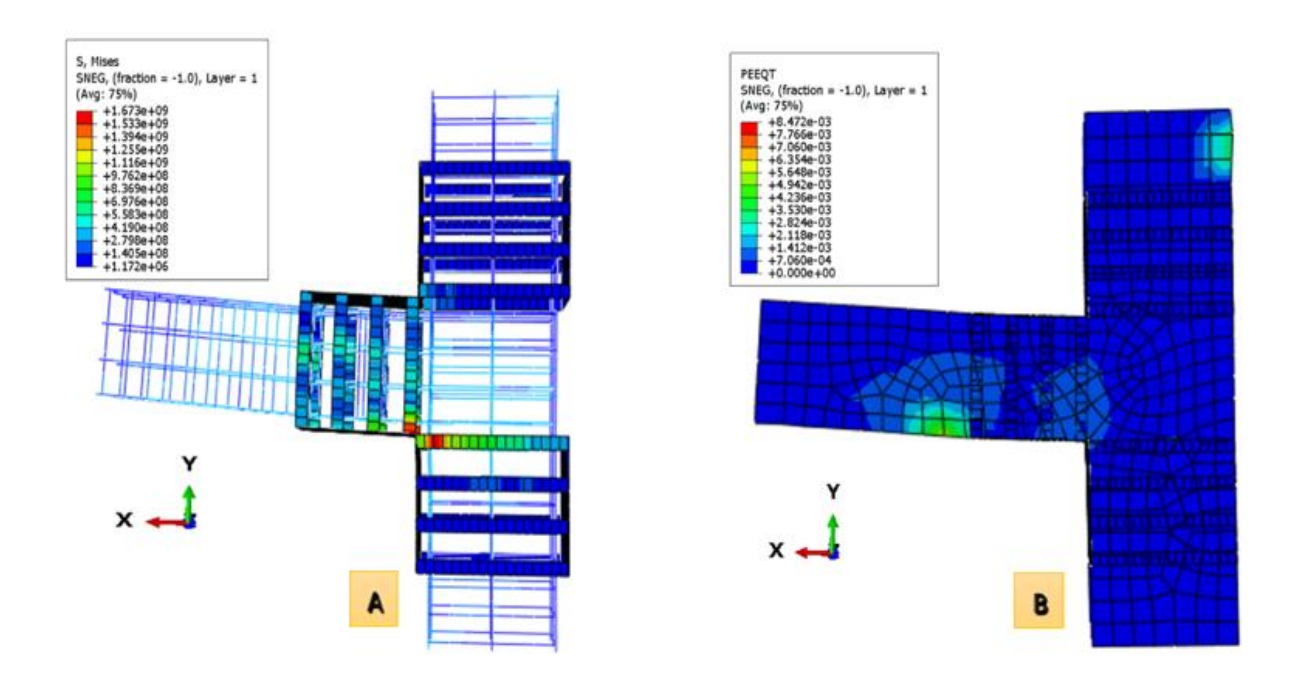


Fig. 18. Comparison between the numerical load-displacement curves for model 1 and numerical analysis.

# 3.6.2. Model 2 (CFRP sheets with strips)

The numerical analysis of Model (2) illustrates the Von Mises stress contour at the failure moment and PEEQT contour, as depicted in Fig. 19. For the joint in Model 2, the benefits of using carbon fiber-reinforced polymer (CFRP) sheets and strips were more evident than using sheets alone in Model 1. The modified joint strength was increased significantly more than in Model 1 by redirecting the damaged area from the nearby column face to the beam region at the end of the carbon sheet, depending on the length of the beam. This improvement can be attributed to the contribution of the strips, in addition to the carbon sheets, in strengthening the joint for both the column and beam. The strips also help absorb the force applied to the model before it penetrates into the concrete and reinforcing bars as tension reinforcement.

Furthermore, the use of strips in CFRP allows for a more flexible behavior and prevents the carbon sheets from separating from the concrete surface. It is noteworthy that using strips also prevents the development of local stresses in the concrete cover, making the confinement behavior for concrete more effective, as illustrated in Fig. 19 (A and B). By installing CFRP sheets with dimensions of (190 x 200) mm and strips with dimensions of (200 x 20) mm for the beam and (250 x 20) mm for the column, a significant improvement in the ultimate capacity of the joint was achieved over the numerical analysis of Model 1, as shown in Fig. 20.



**Fig. 19.** Numerical retrofitting by CFRP for model 2: (A) Von Mises stress contour at the failure moment, (B) PEEQT contour.

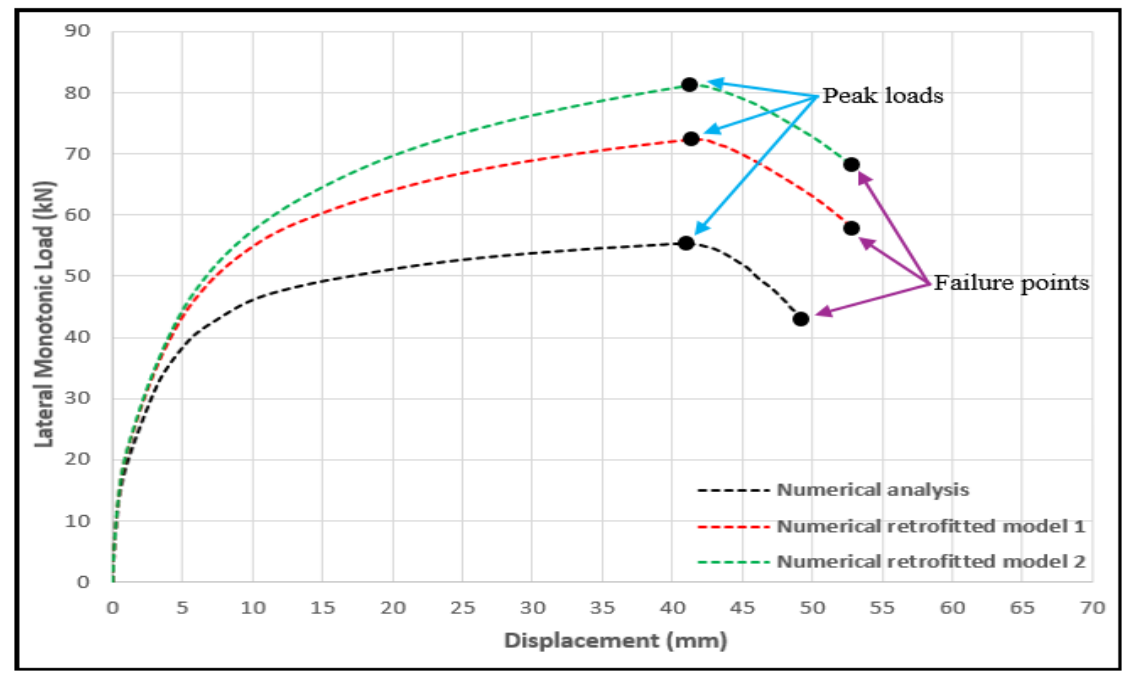


**Fig. 20.** Comparison between the numerical load-displacement curves for model 2 with numerical analysis and model 1.

## 3.6.3. Comparison of Model 1 and Model 2 with Numerical Analysis

Improving the energy dissipation capacity of both unstrengthened and CFRP-strengthened specimens during seismic events is crucial. The results for peak monotonic load (Pp), displacement at peak load (<sup>8</sup>p), energy dissipation (Ediss), and stiffness (K) for numerical models are presented in Table 13. Model 1 showed a significant increase of 30% in peak monotonic load, 25.6% in cumulative energy dissipation, and 29.6% in stiffness compared to the numerical analysis. Model 2 exhibited even higher values, with increases of 47% and 12.3% in peak monotonic load, 36.4% and 8.6% in cumulative energy dissipation, and 45.2% and 12% in stiffness compared to the numerical analysis and Model 1, respectively. These results demonstrate the enhanced energy dissipation capacity of both CFRP-retrofitted specimens, indicating their ability to dissipate energy up to ultimate deformation, as previously verified by researchers [74]. Furthermore, the CFRP retrofitting method significantly improved the stiffness of the retrofitted samples compared to the unretrofitted ones. Prior to retrofitting, the failure mechanism was cracking in the column face near the joint. However, at failure load, debonding occurred between the CFRP sheets and the concrete. The CFRP sheets effectively stopped crack propagation in the column face, shifting the failure to the beam, as also confirmed by previous researchers [75].

K Specimen  $P_p$  $^{\delta}$ p  $E_{diss}$ (kN) (kN-mm) (kN/mm) designation (mm) 1969 55.3 **BCJ-Numerical analysis** 41.0 1.35 72.4 2474 BCJ-Retrofitted model 1 41.4 1.75 BCJ-Retrofitted model 2 81.3 41.4 2686 1.96

Table 13. Numerical Results of cumulative energy dissipation and stiffness for models.

# 4. Statistical analysis

The exterior joint is the most commonly studied type of joint, while the corner joint is the least studied [76]. This is due to the complexity of the structural geometry and less favorable confinement conditions, as exterior beam-column joints are much more vulnerable to seismic loads compared to interior beam-column joints [77,78]. To enhance the exterior joint, the Carbon Fiber Reinforced Polymer (CFRP) strengthening system is the most common due to its advantages.

The number of layers and type of FRP are the main parameters that lead to different failure modes and behaviors. Increasing the number of FRP layers enhances seismic behavior [79,80], but not proportionally to the number of layers [81]. This is due to FRP failure at the joint interface or FRP debonding. It is important to note that increasing the number of FRP layers in the beam region is more effective than in the column region. For different forms of FRP, polymer sheets performed better compared to polymer strips. CFRP has been utilized in various studies, employing different techniques, to enhance the performance of exterior beam-column joints in normal concrete, both in seismic and non-seismic designs, as shown in table 14.

In 2010, Asghar Vatani-Oskouei [82] conducted an experimental study, utilizing CFRP sheets and strips on seismic samples. The results demonstrated a (14.94%) increase in strength for sheets alone and a (19.45%) increase for sheets with strips, compared to the control sample. In 2011, Hamid Sinaei et al. [83] conducted a numerical study, utilizing various techniques of CFRP sheets (top and bottom of the beam, L-shape, U-shape, and both sides) on non-seismic joints. The results showed strength improvements ranging from (6.8 to 14.9) % compared to the control sample, with the most effective technique being CFRP sheets on both sides. In 2014, Varinder Singh et al. [84] conducted an experimental study, utilizing double-layer

X-shaped sheets on a seismic joint. The results showed a (9.50%) improvement in performance compared to the control sample. In 2019, Guo-Lin Wang et al. [85] studied the use of double-layer and three-layer L-shaped sheets around non-seismic joints, resulting in a (19.4%) increase in load-bearing capacity compared to the control sample. Most recently, in 2021, K. Sakthimurugan et al. [51] achieved a (44.7%) improvement in the performance of non-seismic joints by utilizing CFRP sheets and X and L shapes around the joints. In this study, two new numerical techniques of CFRP materials were employed to enhance the performance of seismic joints: sheets and sheets with strips. The results showed a (30%) improvement for Model 1 and a (47%) improvement for Model 2 compared to the reference sample. From these findings, we can conclude that the improvement percentages varied among previous studies and this study due to differences in sample dimensions for the beam and column, concrete compressive strength, and CFRP application techniques in terms of shape and number of layers. However, all results demonstrated a positive impact on joint performance, whether in seismic or non-seismic designs.

**Table 14.** CFRP configurations used in the literature to enhance the load-bearing capacity of beam column joints.

Reference	Type design	Confining CFRP shapes	fc`, MPa	Dimensions (mm)		Peak load (kN)		Percentage
				Beam	Column	before retrofitting	after retrofitting	difference %
Asghar Vatani- Oskouei [82]	SD	Sheets only	24.25	400*350*1780	350*350*2860 -	87.0	100.0	14.94
		Sheets and strips	19.60			92.84	115.26	19.45
Hamid Sinaei et al. [83]	NSD	Sheets top and bottom of beam	- 40 -	300*300*2000	300*300*2300	24.9	27.1	8.8
		L shape					26.6	6.8
		U shape					26.8	7.63
		Both sides					28.6	14.9
Varinder Singh et al. [84]	SD	Sheets with X- shapes (2 layers)	20	125*225*500	225*125*1000	22.68	24.83	9.50
Guo-Lin Wang et al. [85]	NSD	sheets with L shape around joint (2 and 3 layers)	52.8	300*200*1505	300*200*2170	52.1	62.2	19.4
K. Sakthimurugan et al. [51]	NSD	Sheets with X and L shapes	35	300*200*1550	200*200*1440	28.4	41.1	44.7

# 5. Conclusions

The behavior of unreinforced exterior beam-column joint specimens under lateral monotonic loading was investigated experimentally by preparing three test specimens, and then analyzed using the nonlinear finite element program (ABAQUS). Retrofitting the exterior beam-column joint in seismically designed concrete structures using CFRP is considered a relatively new solution and offers significant benefits compared to traditional strengthening techniques. A numerical model with dimensions similar to the experimental specimens was developed and strengthened with carbon fiber. It can be concluded that the CFRP retrofitting technique is highly effective in improving the behavior of concrete connections under lateral monotonic loading. The key findings and observations of the study are summarized as follows:

- The results of the three experimental samples are relatively consistent, with differences between the highest and lowest values of peak monotonic load at (5.4%), cumulative energy dissipation at (2.8%), stiffness at (9.2%), and ductility factor at (15.4%).
- CFRP retrofitting for model 1 improved the performance of the beam-column joint in terms of peak monotonic load, energy dissipation, and stiffness by (30, 25.6 and 29.6) % respectively, compared to the numerical analysis model.
- A significant improvement in peak monotonic load, energy dissipation, and stiffness for model 2 by (47, 36.4, and 45.2) % respectively, compared to the numerical analysis model.
- The retrofitting of the joints using CFRP contributed to reducing deformation under lateral monotonic loads and shifted the failure in the retrofitted numerical models from the column face to the beam body.
- The convergence of the numerical models with the experimental results indicates that the proposed model is entirely accurate.

For future studies, it is recommended to apply the proposed numerical repair methods in this study experimentally on exterior beam-column joint specimens to compare and explore the effectiveness of the reinforcement methods on the seismic and non-seismic performance of the joint. It is also recommended to use two layers of unidirectional carbon fiber reinforced polymer (CFRP) composites and evaluate the performance of the joint after reinforcement.

#### **Abbreviations**

RC	Reinforced concrete	K	Stiffness
fc`	Compressive strength of concrete	μ	Ductility factor
Ac	Surface area of the column section	$P_{y}$	Yield load
${ m P_f}$	First crack load	$^{\delta}_{y}$	Yielding displacement
$^{\delta}{}_{\mathrm{f}}$	Displacement at first crack	$\overset{\delta}{_{u}}$	Effective ultimate displacement
Pp	Peak monotonic load	CDP	Concrete damage plasticity
${}^\delta \! p$	Displacement at peak monotonic load	SD	Seismic design reinforcement
$E_{\rm diss}$	Energy dissipation	NSD	Non-Seismic design reinforcement

# **Funding**

This research did not receive any specific grant from funding agencies in the public, commercial, or not-for-profit sectors.

#### **Conflicts of interest**

The authors declare that they have no known competing financial interests or personal relationships that could have appeared to influence the work reported in this paper.

## **Author's contribution statement**

**Ali Mohammed Owaid:** Conceptualization, Formal analysis, Investigation, Methodology, Software, Validation, Resources, Project administration, Writing - original draft, Writing - review & editing.

Amir Houshang Akhaveissy: Conceptualization, Investigation, Methodology, Supervision, Data curation, Validation; Visualization.

## Bahaa Hussain Al-Abbas: Validation, Supervision.

#### References

- [1] Chu L, Tian Y, Li D, He Y, Feng H. Shear behavior of steel reinforced concrete column-steel beam joints with or without reinforced concrete slab. J Build Eng 2021;35:102063. https://doi.org/10.1016/j.jobe.2020.102063.
- [2] Abdelwahed BS, Kaloop MR, El-Demerdash WE. Nonlinear numerical assessment of exterior Beam-Column connections with Low-Strength concrete. Buildings 2021;11:562. https://doi.org/10.3390/buildings11110562.
- [3] Mosallam A, Allam K, Salama M. Analytical and numerical modeling of RC beam-column joints retrofitted with FRP laminates and hybrid composite connectors. Compos Struct 2019;214:486–503. https://doi.org/10.1016/j.compstruct.2019.02.032.
- [4] Tavasoli E, Rezaifar O, Kheyroddin A. Seismic performance of RC joints retrofitted by external diagonal bolts. J Build Eng 2022;46: 103691. https://doi.org/10.1016/j.jobe.2021.103691.
- [5] Qasem M, Hasan M, Muhamad R, Mutafi A. Non-linear 3D finite element analysis of precast reinforced concrete Beam-Column joint under monotonic static load. Mater Today Proc 2022;65:746–57. https://doi.org/10.1016/j.matpr.2022.03.284.
- [6] Qasem M, Hasan M, Muhamad R. Finite element simulation of precast moment resisting reinforced concrete beam-column joint subjected to monotonic load. Mater Today Proc 2023. https://doi.org/10.1016/j.matpr.2023.03.532.
- [7] Xiao J, Ding T, Zhang Q. Structural behavior of a new moment-resisting DfD concrete connection. Eng Struct 2017;132:1–13. https://doi.org/10.1016/j.engstruct.2016.11.019.
- [8] Vecchi F, Belletti B. Capacity assessment of existing RC columns. Buildings 2021;11:161. https://doi.org/10.3390/buildings11040161.
- [9] Ding T, Xiao J. Behavior of concrete beam-column frame joints with DfD connections: A simulation study with interface modelling. Eng Struct 2019;189:347–58. https://doi.org/10.1016/j.engstruct.2019.03.082.
- [10] Majumder S, Saha S. Quasi-static cyclic performance of RC exterior beam-column joint assemblages strengthened with geosynthetic materials. Structures 2021;29:1210–28. https://doi.org/10.1016/j.istruc.2020.12.010.
- [11] De Santis S, de Felice G, Roscini F. Retrofitting of masonry vaults by basalt textile-reinforced mortar overlays. Int J Archit Herit 2019;13:1061–77. https://doi.org/10.1080/15583058.2019.1597947.
- [12] Saad AG, Sakr MA, El-korany TM. The shear strength of existing non-seismic RC beam-column joints strengthened with CFRP Sheets: Numerical and analytical study. Eng Struct 2023;291: 116497. https://doi.org/10.1016/j.engstruct.2023.116497.
- [13] Barmi CG, Saghafi MH, Golafshar A. Providing a strategy to restore damaged RC beam-column joints with the combination of CFRP and HPFRCC. Eng Struct 2024;299:117148. https://doi.org/10.1016/j.engstruct.2023.117148.
- [14] Tafsirojjaman T, Miri A, Noor-E-Khuda S, Ahmed A, Islam ABMS, Khan M. Structural performance of CFRP strengthened SHS beam-column connections subjected to monotonic loading: A numerical simulation. Structures 2024;61:106030. https://doi.org/10.1016/j.istruc.2024.106030.
- [15] Tomlinson D, Fam A. Performance of concrete beams reinforced with basalt FRP for flexure and shear. J Compos Constr 2015;19:4014036. https://doi.org/10.1061/(ASCE)CC.1943-5614.0000491.
- [16] Chen P-Y, Feng R, Xu Y, Zhu J-H. Recycling and reutilization of waste carbon fiber reinforced plastics: current status and prospects. Polymers (Basel) 2023;15:3508. https://doi.org/10.3390/polym15173508.
- [17] Park S-J, Park S-J. Novel carbon fibers and their composites. Carbon Fibers 2018;210:295–342. https://doi.org/10.1007/978-981-13-0538-2\_9.
- [18] Jahami A, Issa CA. An Updated Review on the Effect of CFRP on Flexural Performance of Reinforced Concrete Beams. Int J Concr Struct Mater 2024;18:14. https://doi.org/10.1186/s40069-023-00651-y.

- [19] Alshamrani S, Rasheed HA, Salahat FH, Borwankar A, Divilbiss N. Seismic flexural behavior of CFRP strengthened reinforced concrete beams secured with fiber anchors. Eng Struct 2024;305: 117728. https://doi.org/10.1016/j.engstruct.2024.117728.
- [20] Cao X, Wang W, Tan X, Zhang Y. Seismic behaviour of pre-damaged RC columns strengthened with CFRP grid/sprayed ECC jackets subjected to horizontal reversed cyclic loading and constant axial force. Case Stud Constr Mater 2024;20: e02948. https://doi.org/10.1016/j.cscm.2024.e02948.
- [21] Zhou J, Hu Z, Wang B, Li X, Han J. Experimental investigation of CFRP-confined partially encased composite columns under axial compression. J Build Eng 2024;81: 108094. https://doi.org/10.1016/j.jobe.2023.108094.
- [22] Farhang K, Farahbod F, Nezamabadi MF, Mansouri B. Shear strengthening of RC 3D exterior beam-column joints with CFRP sheets an experimental and numerical study. Asian J Civ Eng 2023;24:1599–619. https://doi.org/10.1007/s42107-023-00591-8.
- [23] Fan G, Yang J, Liu J, Yang S, Gao M. Research on Seismic Performance of Eccentric Beam-Column Joint Retrofitted with CFRP-Steel Plate. Int J Civ Eng 2024;22:597-617. https://doi.org/10.1007/s40999-023-00919-0.
- [24] El Ghadioui R, Hiesch D, Bujotzek L, Proske T, Graubner C-A. Structural behaviour of CFRP reinforced concrete members under monotonic and cyclic long-term loading. Mater Struct 2021;54:137. https://doi.org/10.1617/s11527-021-01728-4.
- [25] Mohammed AA, Manalo AC, Ferdous W, Zhuge Y, Vijay P V, Pettigrew J. Experimental and numerical evaluations on the behaviour of structures repaired using prefabricated FRP composites jacket. Eng Struct 2020;210:110358. https://doi.org/10.1016/j.engstruct.2020.110358.
- [26] Siddika A, Al Mamun MA, Ferdous W, Alyousef R. Performances, challenges and opportunities in strengthening reinforced concrete structures by using FRPs–A state-of-the-art review. Eng Fail Anal 2020;111:104480. https://doi.org/10.1016/j.engfailanal.2020.104480.
- [27] Mohammed AA, Manalo A, Ferdous W, Abousnina R, AlAjarmeh O, Vijay P V, et al. Design considerations for prefabricated composite jackets for structural repair: Parametric investigation and case study. Compos Struct 2021;261:113288. https://doi.org/10.1016/j.compstruct.2020.113288.
- [28] Akguzel U, Pampanin S. Assessment and design procedure for the seismic retrofit of reinforced concrete beam-column joints using FRP composite materials. J Compos Constr 2012;16:21–34. https://doi.org/10.1061/(ASCE)CC.1943-5614.0000242.
- [29] Tafsirojjaman T, Fawzia S, Thambiratnam DP, Zhao X-L. FRP strengthened SHS beam-column connection under monotonic and large-deformation cyclic loading. Thin-Walled Struct 2021;161:107518. https://doi.org/10.1016/j.tws.2021.107518.
- [30] Ali SA, Forth JP. An experimental and analytical investigation of reinforced concrete beam-column joints strengthened with a range of CFRP schemes applied only to the beam. Adv Struct Eng 2021;24:2748–66. https://doi.org/10.1177/13694332211007371.
- [31] Alshaikh IMH, Nehdi ML, Abadel AA. Numerical investigations on progressive collapse of rubberized concrete frames strengthened by CFRP sheets. Structures 2024;60:105918. https://doi.org/10.1016/j.istruc.2024.105918.
- [32] Del Vecchio C, Di Ludovico M, Prota A, Manfredi G. Analytical model and design approach for FRP strengthening of non-conforming RC corner beam—column joints. Eng Struct 2015;87:8–20. https://doi.org/10.1016/j.engstruct.2015.01.013.
- [33] Dalalbashi A, Eslami A, Ronagh HR. Numerical investigation on the hysteretic behavior of RC joints retrofitted with different CFRP configurations. J Compos Constr 2013;17:371–82. https://doi.org/10.1061/(ASCE)CC.1943-5614.0000361.
- [34] Morankar A, Pisolkar A V. STUDY OF STRUCTURAL BEHAVIOR OF RETROFIT BEAM COLUMN JUNCTION USING ANSYS. I-Manager's J Struct Eng 2023;11:1.
- [35] Wang J, Yue X, Li F, Sun Y, Li Z. Post-Fire Seismic Property of Reinforced Concrete Frame Joints with Carbon Fiber-Reinforced Polymer Using Numerical Analysis. Fire 2023;6:205. https://doi.org/10.3390/fire6050205.

- [36] John F. Bonacci SMA. Recommendations for Design of Beam-Column Connections in Monolithic Reinforced Concrete Structures. Am Concr Institute, ACI 352R-02 2002: 1-37.
- [37] Farmington Hills, MI U. Building Code Requirements for Structural Concrete and Commentary. Am Concr Institute, ACI 318-19 2019:628.
- [38] ASTM A615/AM615-15. Standard Specification for Deformed and Plain Carbon-Steel Bars for Concrete Reinforcement. Am Soc Test Mater 2015.
- [39] Dixon, Donald E., Jack R. Prestrera, George RU Burg, Subcommittee A. Chairman, Edward A. Abdun-Nur, Stanley G. Barton LWB et al. Standard Practice for Selecting Proportions for Normal, Heavyweight, and Mass Concrete. Am Concr Inst (ACI 2111-91) (1991, Reapproved 2002) n.d.
- [40] ASTM C150/C150-07. Standard Specification for Portland Cement. Am Soc Test Mater 2007.
- [41] ASTM C33/C33M-16. Standard specification for concrete aggregate. Am Soc Test Mater 2016.
- [42] ASTM C494/C494-05. Standard specification for chemical admixtures for concrete. Am Soc Test Mater 2005.
- [43] ASTM C143/143-05. Standard Test Method for Slump of Hydraulic Cement Concrete. Am Soc Test Mater 2005.
- [44] Norman L. Scott NMH, Michael E. Kreger LDM. Commentary on Acceptance Criteria for Moment Frames Based on Structural Testing. Am Concr Institute, ACI T11-01 2001.
- [45] Azimi M, Adnan A Bin, Bin Mohd Sam AR, Tahir MM, Faridmehr I, Hodjati R. Seismic performance of RC beam-column connections with continuous rectangular spiral transverse reinforcements for low ductility classes. Sci World J 2014;2014:802605. https://doi.org/10.1155/2014/802605.
- [46] Alhaddad MS, Siddiqui NA, Abadel AA, Alsayed SH, Al-Salloum YA. Numerical investigations on the seismic behavior of FRP and TRM upgraded RC exterior beam-column joints. J Compos Constr 2012;16:308–21. https://doi.org/10.1061/(ASCE)CC.1943-5614.0000265.
- [47] Melo J, Varum H, Rossetto T. Experimental assessment of the monotonic and cyclic behaviour of exterior RC beam-column joints built with plain bars and non-seismically designed. Eng Struct 2022;270:114887. https://doi.org/10.1016/j.engstruct.2022.114887.
- [48] Wang Z, Huang J, Chang Z, Lu Y. Experimental and Numerical Investigation on Seismic Performance of RC Exterior Beam-Column Joints with Slabs. Shock Vib 2022;2022:3679431. https://doi.org/10.1155/2022/3679431.
- [49] Melo J, Pohoryles DA, Rossetto T, Varum H. Full-scale cyclic testing of realistic reinforced-concrete beam-column joints. MethodsX 2021;8: 101409. https://doi.org/10.1016/j.mex.2021.101409.
- [50] Ugale AB, Khante SN. Study of energy dissipation of reinforced concrete beam-column joint confined using varying types of lateral reinforcements. Mater Today Proc 2020;27: 1356-1361. https://doi.org/10.1016/j.matpr.2020.02.690.
- [51] Sakthimurugan K, Baskar K. Experimental investigation on rcc external beam-column joints retrofitted with basalt textile fabric under static loading. Compos Struct 2021;268: 114001. https://doi.org/10.1016/j.compstruct.2021.114001.
- [52] Deng B-Y, Liu X, Yu K-Q, Li L-Z, Chen Y. Seismic retrofitting of RC joints using steel cage and haunch with bolted steel plate. Structures 2022;43: 285-298. https://doi.org/10.1016/j.istruc.2022.06.056.
- [53] Park R. Evaluation of ductility of structures and structural assemblages from laboratory testing. Bull New Zeal Soc Earthq Eng 1989;22:155–66. https://doi.org/10.5459/bnzsee.22.3.155-166.
- [54] Maria AA, Marianovella L, Marisa P. Bond Performances of FRP Rebars-Reinforced Concrete. J Mater Civ Eng 2007;19:205–13. https://doi.org/10.1061/(ASCE)0899-1561(2007)19:3(205).
- [55] Chalioris CE, Kytinou VK, Voutetaki ME, Karayannis CG. Flexural Damage Diagnosis in Reinforced Concrete Beams Using a Wireless Admittance Monitoring System—Tests and Finite Element Analysis. Sensors 2021;21:679. https://doi.org/10.3390/s21030679.
- [56] Moon N. Prediction of blast loading and its impact on buildings 2009.

- [57] Hognestad E, Hanson NW, McHenry D. Concrete stress distribution in ultimate strength design. J Proc 1955;52:455–80.
- [58] Rüsch H. Researches toward a general flexural theory for structural concrete. J Am Concr Inst 1960;57:1–28.
- [59] Kaar PH, Hanson NW, Capell HT. Stress-strain curves and stress block coefficients for high strength concrete. ACI Spec Publ 1978.
- [60] Akhaveissy AH, Desai CS. Application of the DSC model for nonlinear analysis of reinforced concrete frames. Finite Elem Anal Des 2012;50: 98-107. https://doi.org/10.1016/j.finel.2011.09.001.
- [61] Akhaveissy AH, Ali AM, Abbas B. A behavior study of lightweight reinforced concrete deep beams by considering different spacing of stirrups under the effect of fire: Experimental and numerical. J Rehabil Civ Eng 2024;12:137–58. https://doi.org/10.22075/jrce.2023.31484.1889.
- [62] Behnam H, Kuang JS, Huang RYC. Exterior RC wide beam-column connections: Effect of beam width ratio on seismic behaviour. Eng Struct 2017;147: 27-44. https://doi.org/10.1016/j.engstruct.2017.05.044.
- [63] Behnam H, Kuang JS, Samali B. Parametric finite element analysis of RC wide beam-column connections. Comput Struct 2018;205: 28-44. https://doi.org/10.1016/j.compstruc.2018.04.004.
- [64] Zargarian M, Rahai A. Theoretical and Experimental Studies of Two-Span Reinforced Concrete Deep Beams and Comparisons with Strut-and-Tie Method. Adv Civ Eng 2021;2021: 8880067. https://doi.org/10.1155/2021/8880067.
- [65] Soltanabadi R, Behfarnia K, Mamazizi A. Numerical investigation of RC deep beams containing recycled aggregates. Constr Build Mater 2022;324: 126713. https://doi.org/10.1016/j.conbuildmat.2022.126713.
- [66] Chen B, Zhou J, Zhang D, Su J, Nuti C, Sennah K. Experimental study on shear performances of ultra-high performance concrete deep beams. Structures 2022;39: 310-322. https://doi.org/10.1016/j.istruc.2022.03.019.
- [67] Demir A, Caglar N. Numerical determination of crack width for reinforced concrete deep beams. Comput Concr An Int J 2020;25:193–204.
- [68] Dabiri H, Kheyroddin A, Kaviani A. A Numerical Study on the Seismic Response of RC Wide Column–Beam Joints. Int J Civ Eng 2019;17:377–95. https://doi.org/10.1007/s40999-018-0364-2.
- [69] Najafgholipour MA, Arabi AR. Finite-element study on the behavior of exterior reinforced concrete beam-to-column connections with transverse reinforcement in the joint panel. Pract Period Struct Des Constr 2021;26:4020050. https://doi.org/10.1061/(ASCE)SC.1943-5576.00005.
- [70] Spozito RS, Rodrigues EFC, dos Santos HF, de Oliveira IA, Christoforo AL, de Almeida Filho FM, et al. Numerical Modeling of Four-Pile Caps Using the Concrete Damaged Plasticity Model. Buildings 2024;14:2066. https://doi.org/10.3390/buildings14072066.
- [71] Abed F, Oucif C, Awera Y, Mhanna HH, Alkhraisha H. FE modeling of concrete beams and columns reinforced with FRP composites. Def Technol 2021;17:1–14. https://doi.org/10.1016/j.dt.2020.02.015.
- [72] Akhaveissy AH, Permanoon A, Mirzaei M. Seismic Retrofit of Defective RC Beam-Column Joints. Period Polytech Civ Eng 2018;62:596–611. https://doi.org/10.3311/PPci.10661.
- [73] Nagaraja SG, Pletz M, Schuecker C. Constitutive modeling of anisotropic plasticity with application to fiber-reinforced composites. Int J Solids Struct 2019;180–181:84–96. https://doi.org/10.1016/j.ijsolstr.2019.07.002.
- [74] Tafsirojjaman T, Fawzia S, Thambiratnam DP. Structural behaviour of CFRP strengthened beam-column connections under monotonic and cyclic loading. Structures 2021;33:2689–99. https://doi.org/10.1016/j.istruc.2021.06.028.
- [75] Hejazi F, Karim H, Kazemi H, Shahbazpanahi S, Mosavi A. Fracture mechanics modeling of reinforced concrete joints strengthened by CFRP sheets. Case Stud Constr Mater 2022;17:e01273. https://doi.org/10.1016/j.cscm.2022.e01273.
- [76] Pohoryles DA, Melo J, Rossetto T, Varum H, Bisby L. Seismic retrofit schemes with FRP for deficient RC beam-column joints: State-of-the-art review. J Compos Constr 2019;23:3119001. https://doi.org/10.1061/(ASCE)CC.1943-5614.0000950.
- [77] Ghobarah A, Saatcioglu M, Nistor I. The impact of the 26 December 2004 earthquake and tsunami on structures and infrastructure. Eng Struct 2006;28:312–26. https://doi.org/10.1016/j.engstruct.2005.09.028.

- [78] Zhao B, Taucer F, Rossetto T. Field investigation on the performance of building structures during the 12 May 2008 Wenchuan earthquake in China. Eng Struct 2009;31:1707–23. https://doi.org/10.1016/j.engstruct.2009.02.039.
- [79] Hadi MNS, Tran TM. Seismic rehabilitation of reinforced concrete beam—column joints by bonding with concrete covers and wrapping with FRP composites. Mater Struct 2016;49:467–85. https://doi.org/10.1617/s11527-014-0511-4.
- [80] Parvin A, Altay S, Yalcin C, Kaya O. CFRP rehabilitation of concrete frame joints with inadequate shear and anchorage details. J Compos Constr 2010;14:72–82. https://doi.org/10.1061/(ASCE)CC.1943-5614.0000055.
- [81] Antonopoulos CP, Triantafillou TC. Experimental investigation of FRP-strengthened RC beam-column joints. J Compos Constr 2003;7:39–49. https://doi.org/10.1061/(ASCE)1090-0268(2003)7:1(3.
- [82] Vatani-Oskouei A. Repairing of seismically damaged RC exterior beam—column connection using CFRP. J Reinf Plast Compos 2010;29:3257–74. https://doi.org/10.1177/0731684410371407.
- [83] Sinaei H, Jumaat MZ, Shariati M. Numerical investigation on exterior reinforced concrete Beam-Column joint strengthened by composite fiber reinforced polymer (CFRP). Int J Phys Sci 2011;6:6572–9. https://doi.org/10.5897/IJPS11.1225.
- [84] Singh V, Bansal PP, Kumar M, Kaushik SK. Experimental studies on strength and ductility of CFRP jacketed reinforced concrete beam-column joints. Constr Build Mater 2014;55:194–201. https://doi.org/10.1016/j.conbuildmat.2014.01.047.
- [85] Wang G-L, Dai J-G, Bai Y-L. Seismic retrofit of exterior RC beam-column joints with bonded CFRP reinforcement: An experimental study. Compos Struct 2019;224: 111018. https://doi.org/10.1016/j.compstruct.2019.111018.